JOURNAL OF GEOPHYSICAL RESEARCH, VOL. 113, E00A22, doi:10.1029/2008JE003077, 2008

Microscopy capabilities of the Microscopy, Electrochemistry, and Conductivity Analyzer

M. H. Hecht,[1] J. Marshall,[2] W. T. Pike,[3] U. Staufer,[4] D. Blaney,[1] D. Braendlin,[5] S. Gautsch,[4] W. Goetz,[6] H.-R. Hidber,[7] H. U. Keller,[6] W. J. Markiewicz,[6] A. Mazer,[1] T. P. Meloy,[8,9] J. M. Morookian,[1] C. Mogensen,[1] D. Parrat,[4] P. Smith,[10] H. Sykulska,[3] R. J. Tanner,[10] R. O. Reynolds,[10] A. Tonin,[7] S. Vijendran,[3] M. Weilert,[1] and P. M. Woida[10]

Received 16 January 2008; revised 5 May 2008; accepted 24 July 2008; published 31 October 2008.

[1] The Phoenix microscopy station, designed for the study of Martian dust and soil, consists of a sample delivery system, an optical microscope, and an atomic force microscope. The combination of microscopies facilitates the study of features from the millimeter to nanometer scale. Light-emitting diode illumination allows for full color optical imaging of the samples as well as imaging of ultraviolet-induced visible fluorescence. The atomic force microscope uses an array of silicon tips and can operate in both static and dynamic mode.

Citation: Hecht, M. H., et al. (2008), Microscopy capabilities of the Microscopy, Electrochemistry, and Conductivity Analyzer, *J. Geophys. Res.*, *113*, E00A22, doi:10.1029/2008JE003077.

1. Introduction

[2] The Phoenix mission has the prime science goal of ''following the water,'' an essentially astrobiological theme. Understanding the role of water in both paleohydrological and contemporary meteorological contexts provides a means of assessing the potential for Mars to have developed, or perhaps even retain, microbially habitable niches within the near subsurface of the planet. The Microscopy, Electrochemistry, and Conductivity Analyzer (MECA) on Phoenix includes a microscopy element that will be a valuable tool for assessing the role of water within the depth range excavated by the lander's robotic arm (RA). Originally developed for the Mars Surveyor Program 2001 Lander to address issues related to human exploration [*Hecht et al.*, 1999], MECA has been adapted to serve as a geological tool that will provide clues about the role of water in the northern subpolar regions where ice is predicted to be present only centimeters beneath the top regolithic material.

[3] MECA is a suite of three instruments, two fixed on the spacecraft deck and the third mounted as an end effector on the Lander's robotic arm. An enclosure contains the Wet Chemistry Laboratory (WCL), the Microscopy Station, electronics specific to those instruments, and all common electronics. Also in the enclosure are the Power Board and the Command and Measurement Electronics Board (CME). Mounted on the robot arm scoop is a second assembly containing the Thermal and Electrical Conductivity Probe (TECP) and its instrument-specific electronics (Figure 1). This paper describes only the Microscopy Station.

[4] The observational targets of the MECA microscopy system include (1) grain size, (2) grain-size distribution, (3) grain shape (including aggregates), and (4) grain surface texture. Key to selecting representative samples for analysis is a sampling system equipped with ''microbuckets'' to catch grains up to a couple of millimeters in diameter and with substrates designed to capture dilute fields of submillimeter particles using geometric, chemical, and magnetic adhesion. The imaging system couples a modest resolution, fixed magnification optical microscope (OM) with a high resolution Atomic Force Microscope (AFM) to capture the finest of particle features.

[5] The Phoenix landing site is expected to be a region of cryoturbationally processed impact ejecta mixed with wind-blown sand and dust from distant sources. The regolith grains will exhibit features inherited from the pre-impact provenance of the material, but cryoturbation and impact can affect grain shape and texture, and can introduce grain sorting effects. Impact, for example, can enhance grain angularity, and while there are no studies of the surface textural response of grains to cryoturbational processes, it might reasonably be expected to enhance rounding as grains

[1]Jet Propulsion Laboratory, California Institute of Technology, Pasadena, California, USA.
[2]SETI Institute, Mountain View, California, USA.
[3]Department of Electrical and Electronic Engineering, Imperial College, London, UK.
[4]Institute of Microtechnology, University of Neuchâtel, Neuchâtel, Switzerland.
[5]Nanosurf AG, Liestal, Switzerland.
[6]Max Planck Institute for Solar System Research, Katlenburg-Lindau, Germany.
[7]Department of Physics, University of Basel, Basel, Switzerland.
[8]College of Engineering and Mineral Resources, West Virginia University, Morgantown, West Virginia, USA.
[9]Retired.
[10]Lunar and Planetary Laboratory, University of Arizona, Tucson, Arizona, USA.

0148-0227/08/2008JE003077$09.00

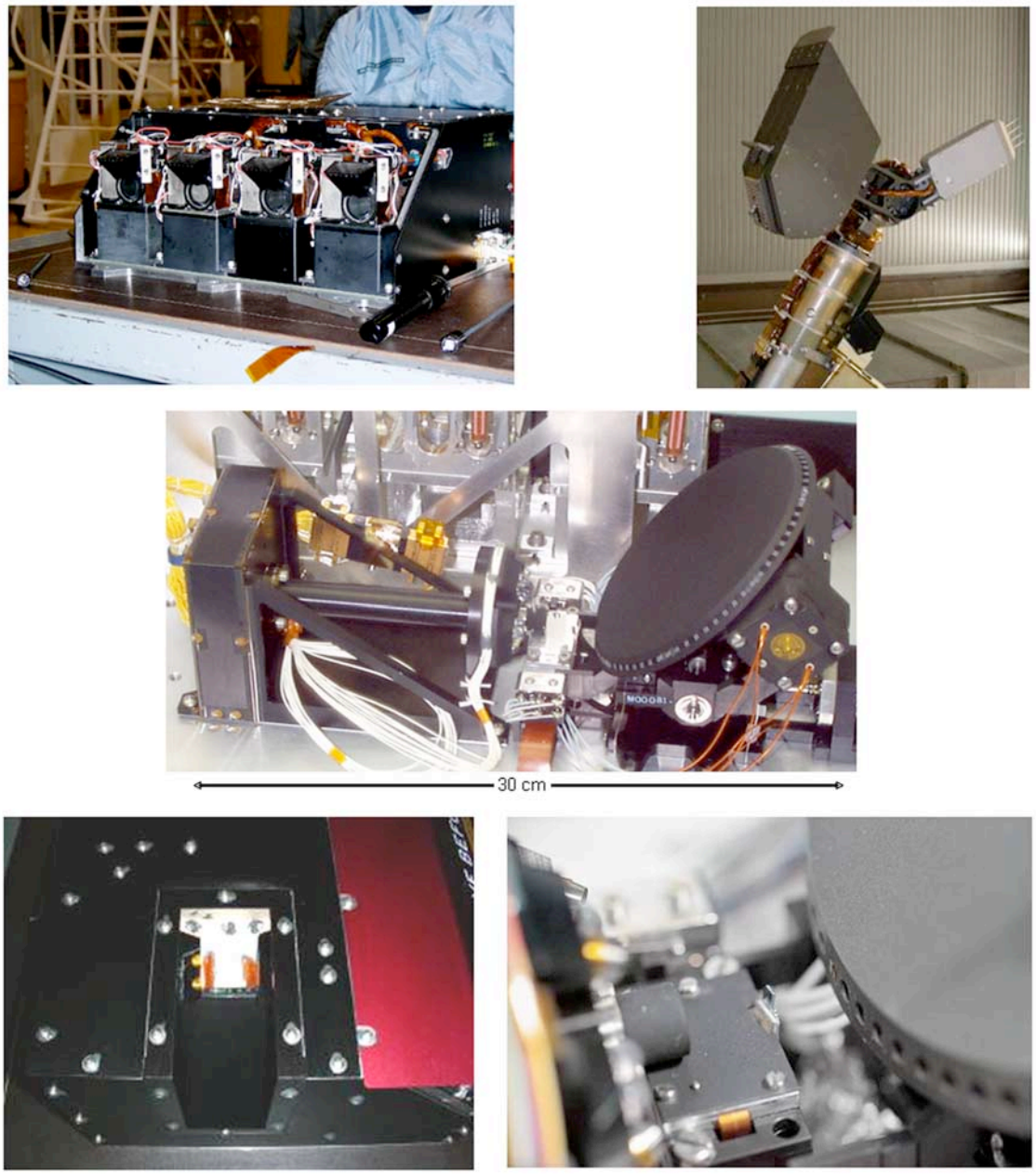

Figure 1. (top left) MECA wet chemistry cells installed in flight enclosure. (top right) TECP mounted on the robotic arm. (middle) The SWTS translates in and out to collect samples, remove excess material, focus, and approach the AFM. It rotates to select any of 69 substrates. (bottom left) The sampling chute, viewed from the top with six substrates exposed. (bottom right) AFM installed under the nose of the optical microscope.

are slowly forced past one another in the polygonal patterns of movement.

[6] The observation of grain cementation, authigenic crystal growth, chemical etching of grains, subduing of grain morphologies, and growth of minerals such as clays and other hydration products would suggest the diagenetic effects of standing water and moisture in the regolith. In the unlikely event that extensive rounding is observed in a grain population, running water might be implicated (aeolian rounding notwithstanding). Running water also leads to sorting of grain sizes, as well as the deposition of sedimentary layers with grading and cyclic characteristics.

[7] Although the sample examined by the microscope system is very small (<10 mg), it has been shown in the laboratory that the judicious combination of microbucket collection and magnetic and regular substrate adhesion can provide a reasonable assessment of grain size distribution. For example, it is possible to determine if a sample is predominantly arenaceous or argillaceous in size, and if there is any bimodality to the grain size distribution. Moreover, the strategy of Phoenix is to assess the full

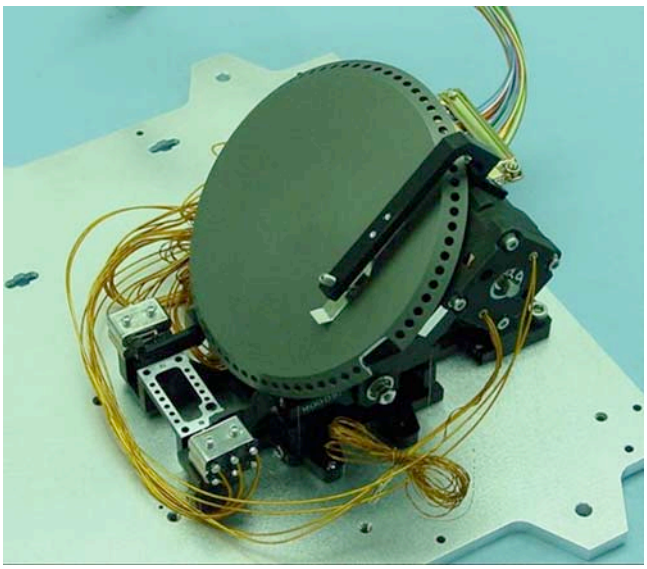

Figure 2. Substrates are arrayed around the beveled edge of the wheel such that they are horizontal for sample delivery and vertical for imaging. A finger has been added to the MSP'01 design to eliminate potential jitter due to play in the gears.

geological context of the landing site by employing several complementary scales of observation. The Surface Stereo Imager (SSI) will visually assess the macroscopic aspects of the landing site –basic geomorphology and geology at the multimeter scale. The Robotic Arm Camera (RAC) will provide the next level of detail ranging from meters down to millimeters. MECA microscopy then provides even greater detail between the millimeter and submicron scales. Ultimately, we intend to conduct grain size analysis on samples by melding data sets from SSI, RAC, OM, and AFM that collectively cover several orders of magnitude in grain size, providing an optical macro- and micro assessment of the landing site.

2. History and Heritage

[8] MECA was originally developed for the Office of Human Exploration and Development of Space (HEDS) as a payload on the 2001 Mars Surveyor Program (MSP'01) lander under the name "Mars Environmental Compatibility Assessment." Bound for an equatorial landing site, MSP'01 was first conceived as an MER-like rover mission until the HEDS office proposed converting the lander deck from a passive deployment platform to an active, but fixed experimental station.

[9] The HEDS payloads addressed both demonstration of essential technology such as conversion of atmospheric CO_2 to O_2 for use as fuel, and investigation of hazards to human exploration, particularly those associated with radiation and dust. MECA was designed to address the latter objective, with components to study the physical and mechanical properties of dust through microscopy (with emphasis on adhesion, abrasion, and inhalation hazards) [*Marshall et al.*, 1999a, 1999b], the possible toxic or corrosive properties of dust through a soluble chemistry experiment, and the electrostatic and triboelectric properties through an electrometer attached to the heel of the robot arm. A fourth MECA component, the "Patch Plate" was a long-term materials exposure experiment.

[10] The MSP'01 MECA instrument was delivered early in 2000, essentially complete except for software but with an abbreviated testing schedule and little operational planning. The mission itself was canceled in the wake of the loss of Mars Polar Lander, and MECA was mothballed for a future opportunity. That opportunity took the form of the Phoenix Scout mission, which is sending the residual MSP'01 platform to a polar destination with a mandate to explore icy terrain in order to elucidate the longterm hydrological cycle on Mars and to search for indications of habitability. Work on the Phoenix implementation began early in 2004.

[11] In adapting MECA to Phoenix, the Patch Plate and Electrometer experiments were abandoned entirely, the latter replaced by the TECP. The WCL experiment was extensively modified to allow it to quantitatively survey the major ionic content and chemical state of a soil-water solution, rather than specifically seeking toxic and corrosive agents. The Microscopy Station, however, was largely unchanged except for an exchange of substrates and removal of an abrasion tool. The original HEDS substrate sets emphasized hardness testing (scraping particles against quartz and glass), soil interaction with engineering materials, and adhesion mechanisms. For Phoenix, only the adhesion experiments were retained, while new substrates were added to allow better examination of bulk samples.

3. Overview

[12] As implemented for both MSP'01 and Phoenix, MECA's Microscopy Station has the following three elements: (1) a sample wheel and translation stage (SWTS), (2) an Optical Microscope, and (3) an Atomic Force Microscope for imaging at the sub-micrometer level (Figure 1) [*Pike et al.*, 2001; *Gautsch*, 2002]. The OM and all supporting electronics were unchanged for Phoenix except for a build-to-print replacement of the illumination system to correct a minor flaw in the grounding scheme. Improvements in the suspension system for the AFM led to a replacement of the sensor head itself, but no changes to the electronics except for an update of the microcode for the embedded processor. Originally developed by Surface/Interface, Inc. (now Transfer Engineering and Manufacturing), the SWTS for Phoenix underwent an overhaul to improve lubrication, replace worn bearings, and reduce a tendency to bind in rotation that resulted from overly tight tolerances in the anti-backlash bearings. The only visible manifestation of the change is a "finger" that presses on the wheel to suppress chatter, compensating for the additional play added to the gear train. In addition, the substrate selection has been changed, and additional baffling has been added to the sampling aperture in the external enclosure to reduce the risk of cross-contamination.

[13] Sample acquisition, OM focusing, and AFM approach are all achieved by translation of the SWTS, while selection of the 69 microscopy substrates is accomplished by SWTS rotation (Figure 2). The 3-mm diameter substrates include 10 sets of six standard coupons, and a utility set of

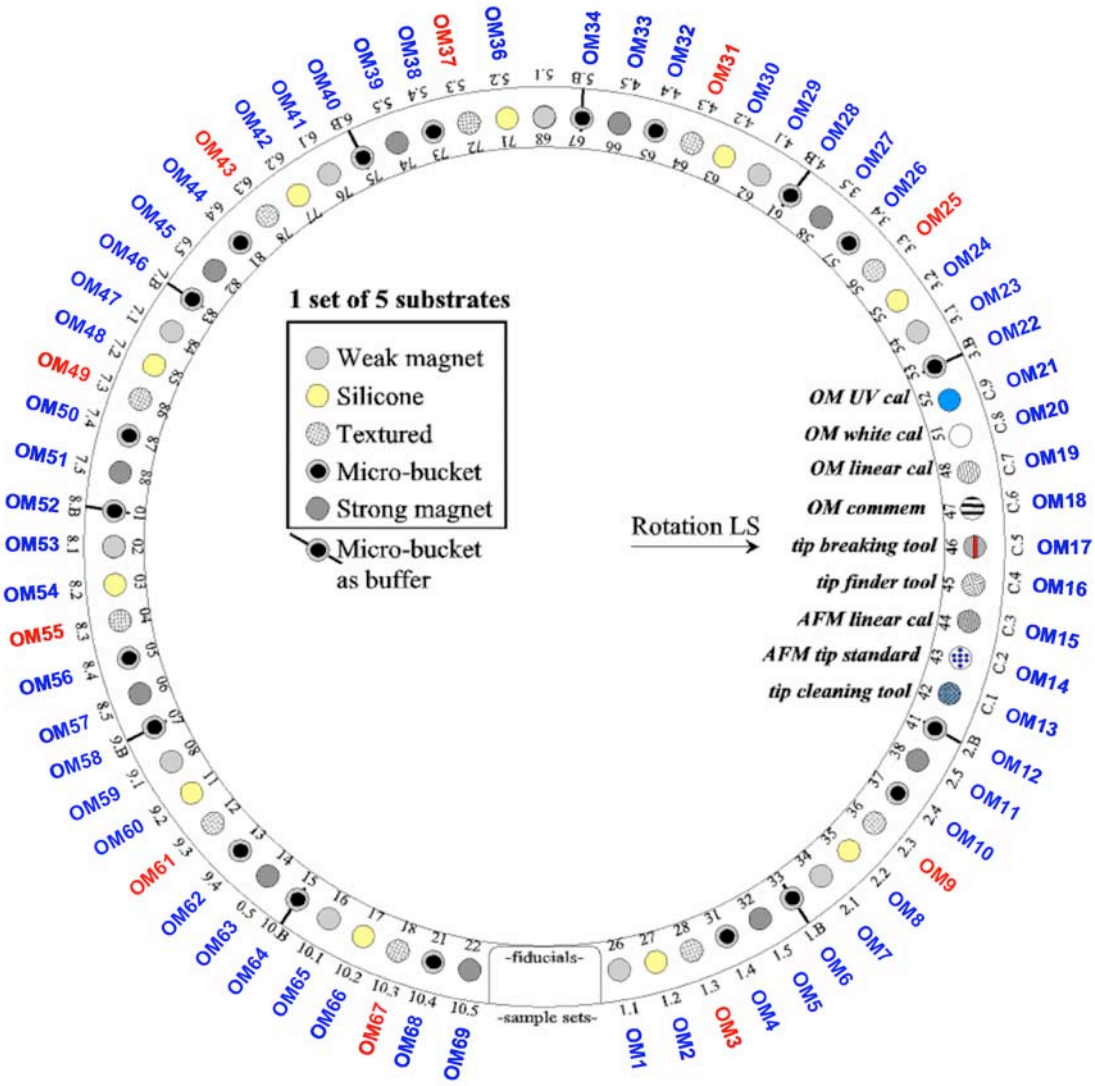

Figure 3. This substrate map for the flight model SWTS shows 10 sets of 6 substrates and 9 calibration substrates.

9 tools and calibration standards (Figure 3). Designed to promote different kinds of particle adhesion, each set of coupons includes a micro-machined silicon target, a weak and a strong magnet, a ''sticky'' silicone disk, and two microbuckets for bulk sampling.

[14] An unusual feature of the MECA Microscopy Station is the positioning of substrates around a 45° bevel on a wheel which is itself mounted at a 45° angle relative to the horizontal. The result is a horizontal loading position and a vertical imaging position such that excess material will fall off the substrates under the influence of gravity. This approach makes it possible to deposit large amounts of material from the Phoenix robot arm scoop while still presenting a relatively sparse field of particles for imaging. Moreover, the SWTS requires only two degrees of freedom to rotate any of 69 substrates between the horizontal load and vertical imaging positions or to translate them to the load, OM focus, and AFM scanning positions.

[15] The OM is the product of a collaboration between the University of Arizona, which developed the optical and illumination system, the Max Planck Institute for Solar System Research (MPS), which provided the CCD and image processing electronics, and the Jet Propulsion Laboratory, which was responsible for mechanical, electronic, and software integration. With heritage from the Pathfinder and MVACS cameras (which it shares with the Beagle 2 Optical Microscope [*Thomas et al.*, 2004]), the OM uses light emitting diodes (LEDs) in four colors for sample illumination, and the fixed-focus 6*x* optics (4 μm/pixel) is a compromise between resolution and depth-of-field. Sharing the Robot Arm Camera (RAC) electronics, the OM's CCD array acquires a 1 × 2 mm image. The array is intrinsically a 512 × 512 frame transfer device that uses half the array (256 × 512) for image collection and the other ''blind'' half to transfer the acquired image, effectively providing a single-clock-cycle electronic shutter [*Kramm et al.*, 1998]. The OM envelope is approximately 7 × 8 × 14 cm and it weighs only 376 g, exclusive of electronics.

[16] The AFM was developed by a Swiss consortium led by the University of Neuchâtel and including the University

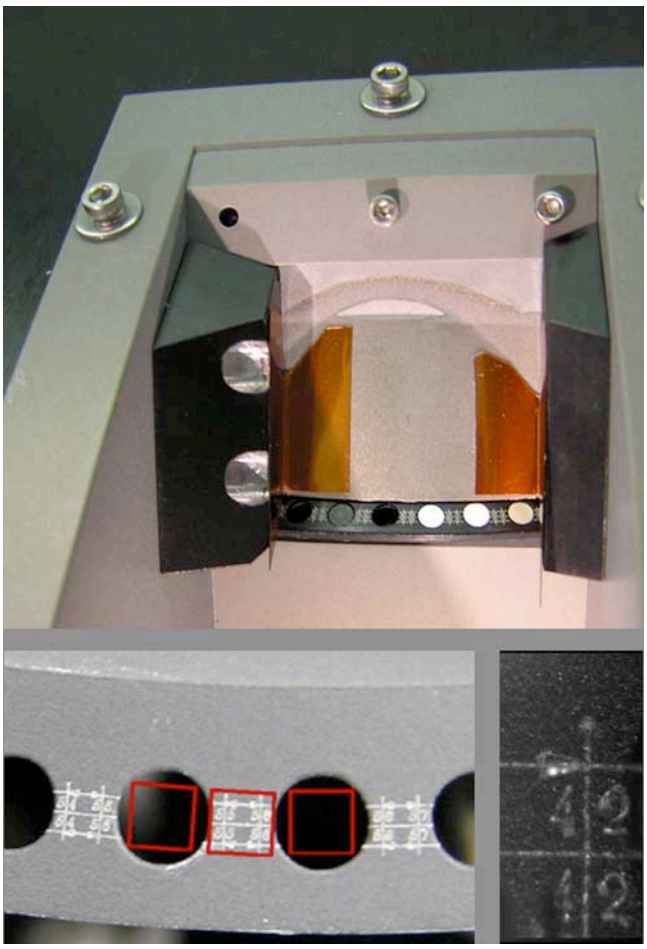

Figure 4. This picture of the extended SWTS was acquired just before final installation of MECA on the flight deck. It shows six exposed substrates. Baffling was added in the form of Kapton tabs to intercept particles that would otherwise contaminate adjacent substrates. (bottom left) A close-up of a segment of the wheel prior to installation of the substrates, showing the 2 × 2 mm frame that would be captured by adjacent 2 × 1 mm images. (bottom right) A close-up of the laser-scribed fiducials between substrates.

of Basel and NanoSurf, AG. Based on a commercial instrument from NanoSurf, the sensor head uses electromagnetic (voice coil) actuators that, compared to conventional piezoelectric drives, operate at low voltages and are relatively insensitive to thermal fluctuations. Controlled by a dedicated microprocessor, the AFM uses a micromachined tip array, and can address a 65 μm square area, an improvement on the 53 μm range for the MSP'01 instrument [*Gautsch*, 2002]. The AFM will typically be used to view particles in the 1–10 μm range and to resolve features larger than 50 nm. While AFMs are capable of resolving much smaller features, below a certain size it becomes difficult to distinguish between mechanical and chemical features. Moreover, interactions with the spacecraft are typically once per day, and on this schedule it is impractical to plan the series of progressively smaller images necessary to maintain a sense of context while zooming in on a feature of interest. A silicone pad in the tool set on the SWTS is used to clean fouled tips, and another tool cleaves off beams with irrecoverable tips to expose the next fresh cantilever.

[17] To operate the Microscopy Station, samples are deposited from the Robotic Arm (RA) to a segment of the wheel that has been translated by the SWTS to protrude out of a horizontal slot in the MECA enclosure (Figure 4). A scraping blade removes excess material as the wheel is withdrawn into the enclosure. The wheel is rotated to select substrates for imaging. In addition to loading, SWTS translation is used for focusing and AFM approach. During operation, the surrounding electronics keep the OM lenses warmer than the outside of the enclosure such that accumulation of water vapor from sublimating icy samples should not cause image degradation.

[18] The MECA Microscopy Station electronics consist of three separate boards which are commanded by the Lander central computer, or command-and-data management system (CDMS). The sample handling system is controlled by a board within the MECA enclosure incorporating a field-programmable gate array (FPGA) able to accept serial commands from the CDMS. The FPGA controls the stepper-motor drives on the SWTS with appropriate responses derived from a series of limit switches. This board also controls the LEDs for the optical microscope. A second board within the MECA enclosure drives the AFM under serial command from the CDMS. As well as its own FPGA, this board also incorporates a dedicated microprocessor with its own operating software. A third board within the warm electronics box of the Lander, shared with the Robotic Arm Camera, drives the OM CCD. This board has a fast serial link to the CDMS and is nearly identical to that used on Mars Polar Lander. A set of software resident on the CDMS integrates the commanding to and data returned from the three MECA boards. This software incorporates several layers of error detection and fault protection for the autonomous operation of the Microscopy Station on Mars, with only occasional daily commanding from Earth.

4. Implementation Considerations

[19] A proper laboratory microscopy investigation of Martian soil would begin with sample preparation, such as separation of particles into different size ranges, followed by mounting of sparse fields of particles on appropriate substrates for viewing with optical and electron microscopes. The optical microscope would optimize the illumination scheme for color contrast and could include the introduction of polarizing and other filters. A stereo microscope would likely be used for better perception of topographic information, and a continuous zoom would provide context for high magnification images. At highest magnification, where depth-of-field is shallow, features would first be observed by scanning the focal plane through the object of interest, possibly by confocal microscopy, combining the series of images into a single, in-focus composite. After suitable bonding to a substrate and sputter-coating to increase electrical conductivity, an electron microscope might be used to continuously zoom and pan into submicron features, with variable stage angles available to further capture the three dimensional character of the particles. The investiga-

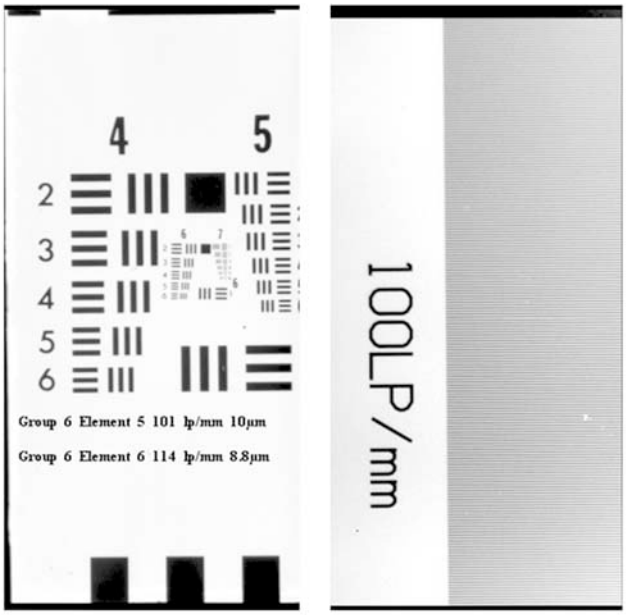

Figure 5. (left) EM OM calibration image of USAF 1951 standard target. (right) FM image of 0.01 mm line width Ronchi ruling.

tion might then be enhanced by energy dispersive X-ray analysis of microscopic features.

[20] Resource constraints on a Mars mission demand an approach that is not only greatly simplified with respect to the one described, but is without precedent in laboratory experience. As a result, it is difficult to rely on literature or even expertise to determine whether a particular subset of capabilities is adequate to capture the scientific objectives of the mission, and a combination of laboratory characterization and intuition is needed to develop a strategy that will yield scientific results of value.

[21] The resource constraints referred to include the obvious limitations of mass, volume, power, data volume, and money. More subtle and often more insidious are the limitations imposed by autonomous operation and the overriding need to minimize risk, both exacerbated by the extreme environments of launch and ground operations. The result is an exceedingly conservative approach to technology (hence, for example, the low density CCDs used here) and avoidance of the use of moving parts such as color filter wheels or zoom lenses. Even with advanced robotics, these constraints make the kind of sample preparation described above entirely impractical.

[22] Of concern in the design of the Microscopy Station was the ability to characterize size, shape, and surface texture of particles over the widest possible size range, while recognizing that the range above ~0.1 mm is better handled by the Phoenix Robot Arm Camera. The design result was a heritage-rich, fixed-focus microscope of modest resolution, relatively large depth of field, and multicolored illumination. To prepare a sparse sample, the SWTS relies on the combination of motion past a fixed blade and a vertical imaging orientation.

[23] The MECA Microscopy Station is part of an imaging strategy that extends from a planetary scale to a submicron scale. Phoenix' Surface Stereo Imager provides the geographic context for the Phoenix excavation, complemented by high resolution orbital imagery from the HiRise instrument on MRO. The excavated material itself is characterized by the Robotic Arm Camera (RAC) which, at a best-resolution of 30 μm per pixel, can resolve particles and features smaller than 0.1 mm inside the robot arm's scoop. The resolution of the RAC is similar to that of the Microscopic Imager on MER, a practical resolution for a "hand-lens" type instrument that needs to be transported to the sample. The MECA Microscopy Station is closer to a true microscope in that it rests on a stable platform in a darkened enclosure with controlled illumination, and samples are prepared in a rudimentary way on the equivalent of a microscope slide. This preparation cannot be without influence on the sample distribution, and therefore coarser features are best viewed in bulk with the RAC. Accordingly, the MECA microscope is optimized for particles and features smaller than 0.1 mm. A substrate size of 3.0 mm was chosen to allow an ensemble of 0.1 mm particles to be scattered in a sparse field, while still providing a sufficient number of substrates to allow for the analysis of many samples.

[24] The optical magnification of the OM was chosen to allow imaging of most of the 3-mm diameter substrate with the heritage 512 $\times$ 256 CCD, while providing sufficient overlap with the field of view of the AFM to allow

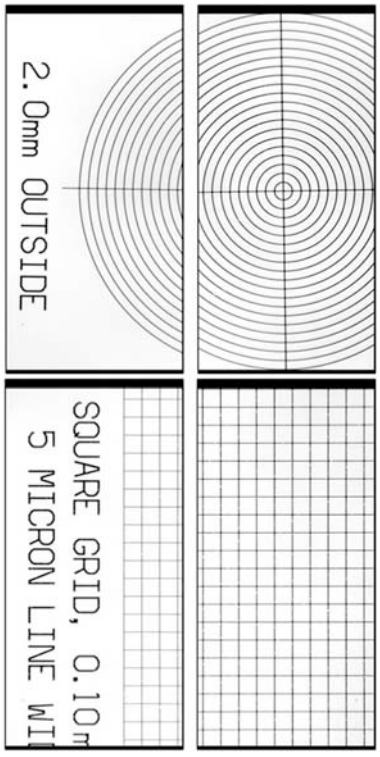

Figure 6. (top left) Flight model OM image of target with 2.0 mm OD, 0.1 mm increments, 7.5 μm line width, positioned to show label. (top right) The same target centered in the field. (bottom left) Flight model OM image of square grid with 0.1 mm spacing, 5 μm line width. (bottom right) The same target centered in the field.

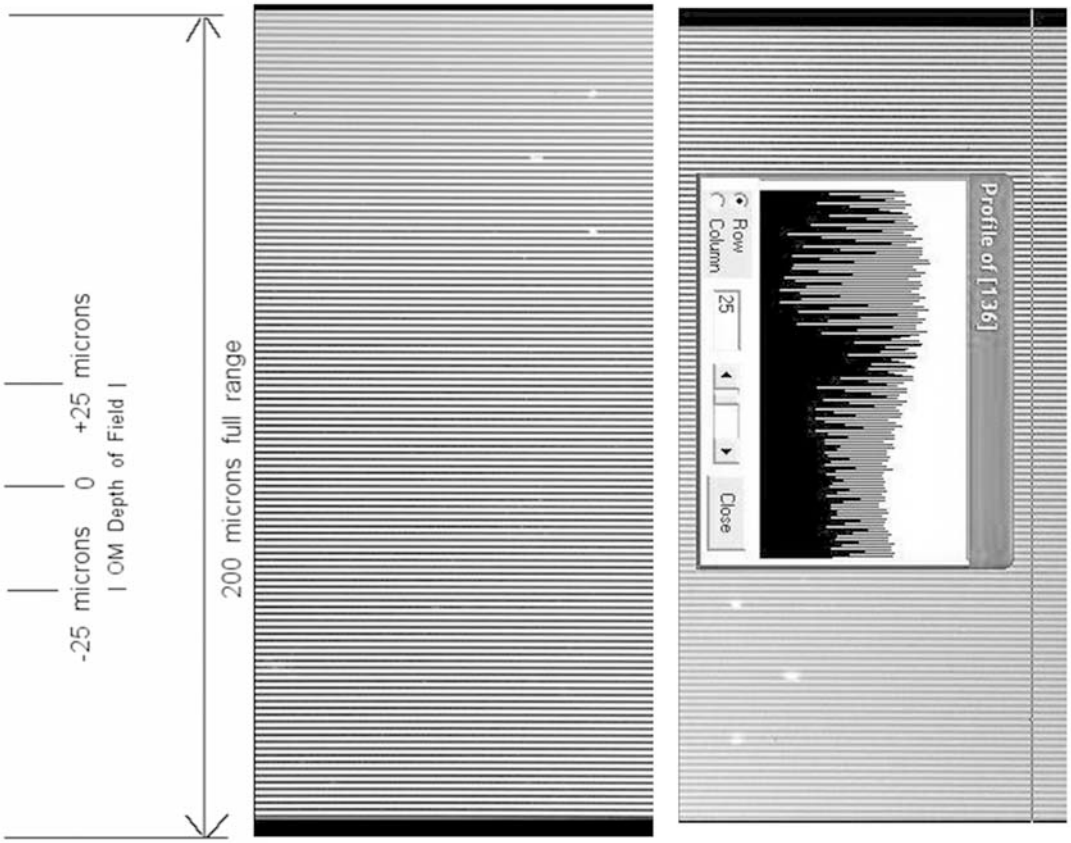

Figure 7. Flight model images of a 60 line pairs/mm Ronchi Grating (16.67 μm period and 8.33 μm line width) angled at 10:1 such that the top of the image is 200 μm below the bottom across the 2 mm FOV. (left) Annotated image of grating with best focus in center. Good resolution and contrast is evident at the ±25 μm marks. (right) Grating translated to focus at the extreme top to show the full range from focus to +200 μm. Modulation transfer function analysis is superimposed.

registration of common features. Additionally, it was chosen to maintain a depth-of-field that is larger than most of the particles likely to be imaged. The result was a 6*x* magnification, 4 μm per pixel (23 μm pixels), which is limited by the pixel size rather than the optical resolution. Pragmatically, this implies a resolution of ~8 μm as compared with the RAC resolution of ~60 μm (30 μm per pixel). The depth of field is between 50 and 100 μm. To capture a pile of particles, the SWTS acquires a through-focus series of several images while translating the optimal focus toward from the substrate surface.

[25] The 2 × 1 mm field of view follows from the selection of the detector and the magnification factor for the optics. Since the image can be shifted laterally by rotation of the wheel, the "portrait" orientation maximizes the total area that can be imaged. A complete, 2 mm high image mosaic covering the entire perimeter of the wheel can be acquired by rotating the wheel 1 mm at a time between images. An adjacent pair of 1 × 2 mm images captures a 2 × 2 mm square, the largest that can be fully inscribed inside each 3 mm diameter substrate (Figure 4).

[26] The role of the MECA AFM is to extend the range of resolution of the OM without sacrificing an inordinate amount of depth-of-field. MECA's AFM extends the resolv-

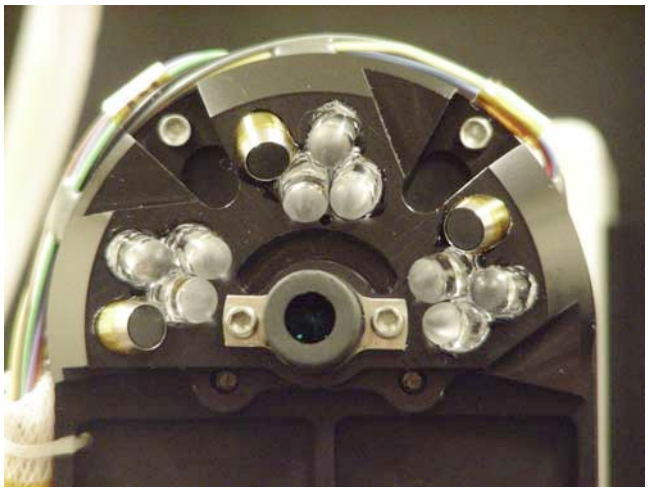

Figure 8. The LED arrangement on the OM. Each cluster contains a red, green, blue, and UV LED (the UV LEDs are in the metal cans).

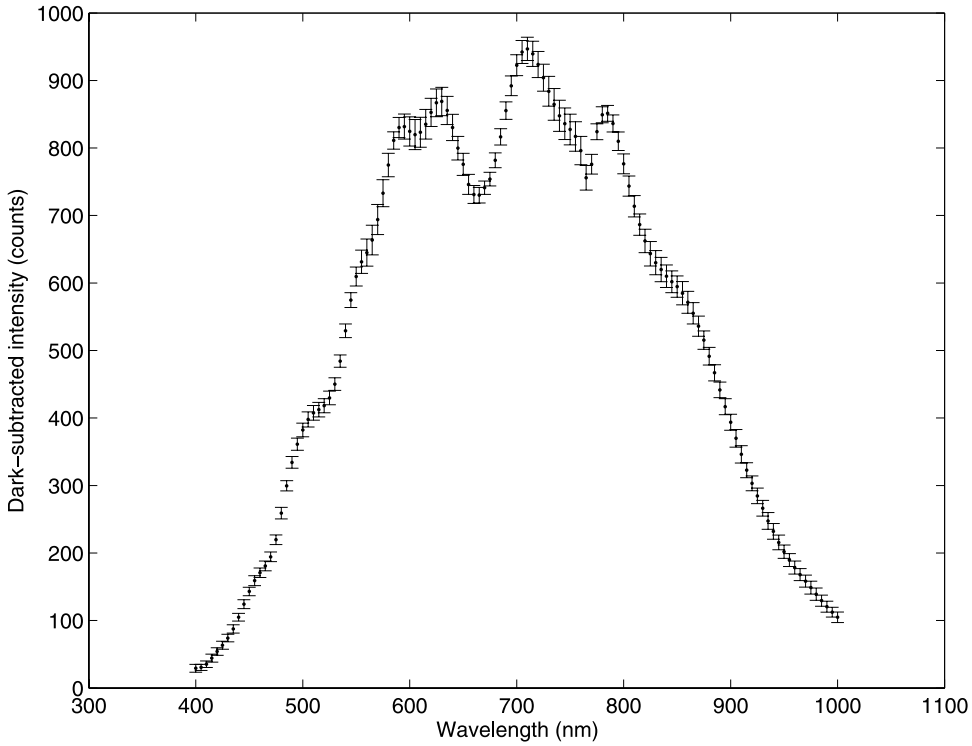

Figure 9. Engineering model OM spectral response.

able range from the ∼6 μm limit of the OM to approximately 0.1 μm while retaining the ability to capture topographic features as tall as 13 μm. Moreover, the AFM can scan a field as wide as 65 μm (in which case the vertical range is reduced to 8 μm), an order of magnitude larger than the smallest feature resolvable by the OM, and thus OM images from one operational day can be used to select AFM targets for subsequent days. This approach is in sharp contrast to laboratory use, where the AFM is typically used to record topography with a resolution of 1–10 nm per

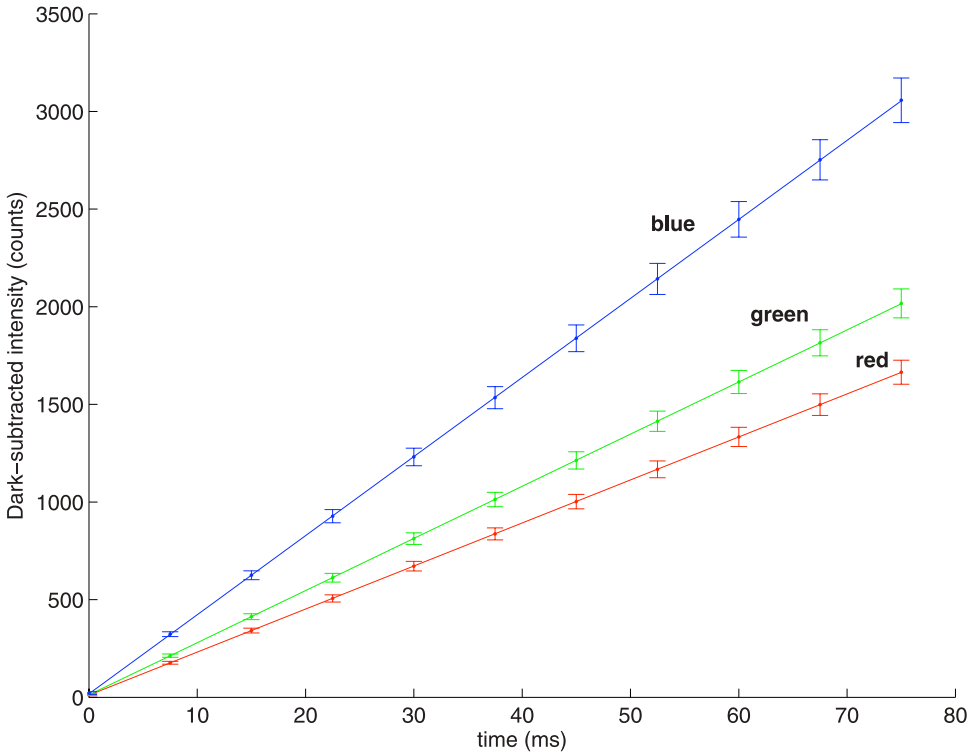

Figure 10. Linearity as a function of exposure time with red, green, and blue LEDs.

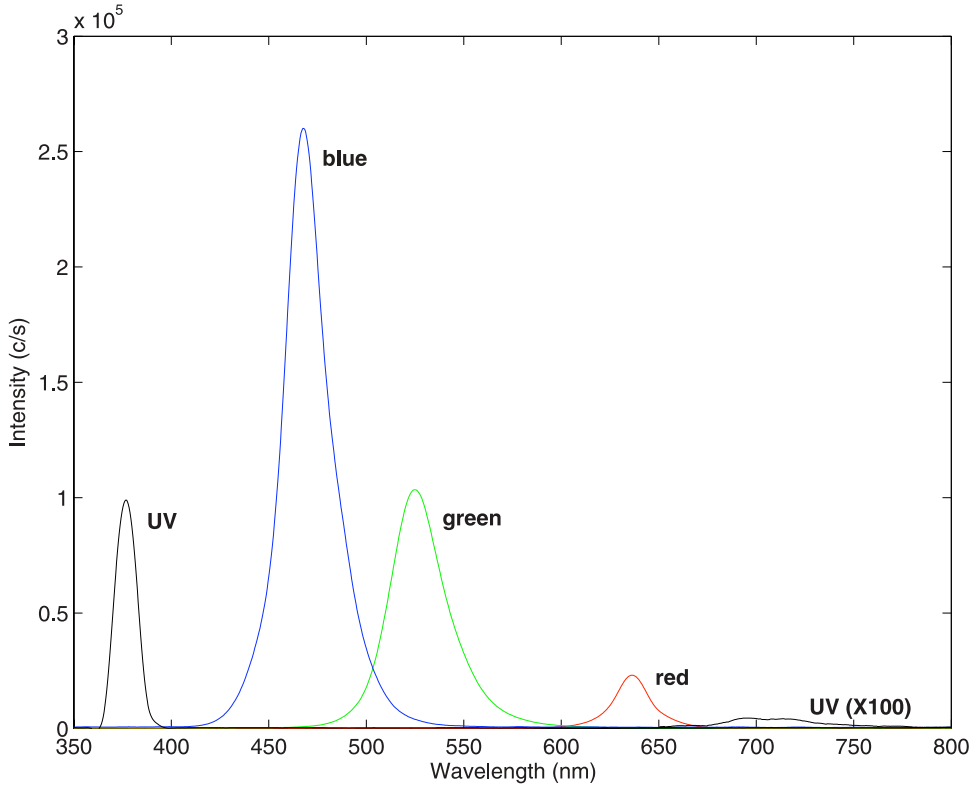

Figure 11. EM OM LED composite spectral output as determined by the Ocean Optics USB2000 spectrometer. The UV LED has a weak visible tail that is blocked by a filter, except for the region around 700 nm.

"pixel" (used loosely here to refer to an element of a topograph) over submicron small areas of flat surfaces. Our laboratory characterization has, however, confirmed that the AFM is capable of meeting these modest performance specifications in a particle-rich environment without excessive tip-particle interactions.

5. Optical Microscope

[27] The MECA optical microscope is a fixed-focus, fixed magnification optical system that sits in a horizontal orientation with a housing in the front containing two lenses surrounded by three banks of four LEDs – one each in red (636 nm), green (543 nm), blue (466 nm), and ultraviolet (375 nm) – and a CCD assembly in the rear. Since the CCD itself is monochrome, color imaging is simulated by combining images acquired with red, green, and blue illumination. The UV LEDs are filtered with a visible light blocking filter (Schott UG-11) and are used for fluorescence measurements only. The CCD is fitted with a 1 mm thick Schott GG420 filter to ensure that it is blind in the passband of the UV light-emitting diode.

[28] The Loral CCD is a 512 pixel square, with 512 × 256 pixels exposed for imaging and the remainder used for frame-transfer. Transfer of image charge to the storage section takes 0.5 ms and does not cause any measurable image degradation for the OM. The active pixel area is 17 × 23 μm, with a 23 μm pixel pitch. The rectangular area results from the incorporation of anti-blooming gates, which run vertically along the array. The CCD was mounted on a custom sensor head board by the Max Planck Institute for Solar System Research (MPS) and provided along with frame-buffering electronics to the University of Arizona for incorporation into the microscope as a contribution to the Phoenix mission.

[29] Electronics for the CCD are shared with the Robot Arm Camera [*Keller et al.*, 2008]. The chip is read out with a 12-bit analog-to-digital converter to provide an image data range of 0–4095 digital numbers (DN). Separate MECA electronics power the LEDs and the sample stage.

[30] Prior to integration, the optical microscope was calibrated using custom rulings, targets, and integrating spheres to determine focal plane response and flat field correction, dark current levels, geometrical parameters (working distance, depth of field, and field of view) and the spectral output of the LEDs. While some of these parameters can be verified on the surface of Mars, it is generally assumed that these properties will not change significantly over the life of the instrument.

[31] Both in the laboratory and on Mars, a white substrate is used to calibrate the intensity and uniformity of each red, green, and blue LED, and a fluorescent substrate (provided by the University of Copenhagen) is used to calibrate the UV LEDs. The 10 μm line of the USAF 1951 standard shown in Figure 5 (group 6, line 5) is readily resolved by the EM, as is the 10 μm separation of a precision Ronchi ruling, suggesting a resolution better than 10 μm.

[32] Field of view and possible spherical or astigmatic aberrations were studied using concentric circle targets. Figure 6 shows the target used for calibration of the flight

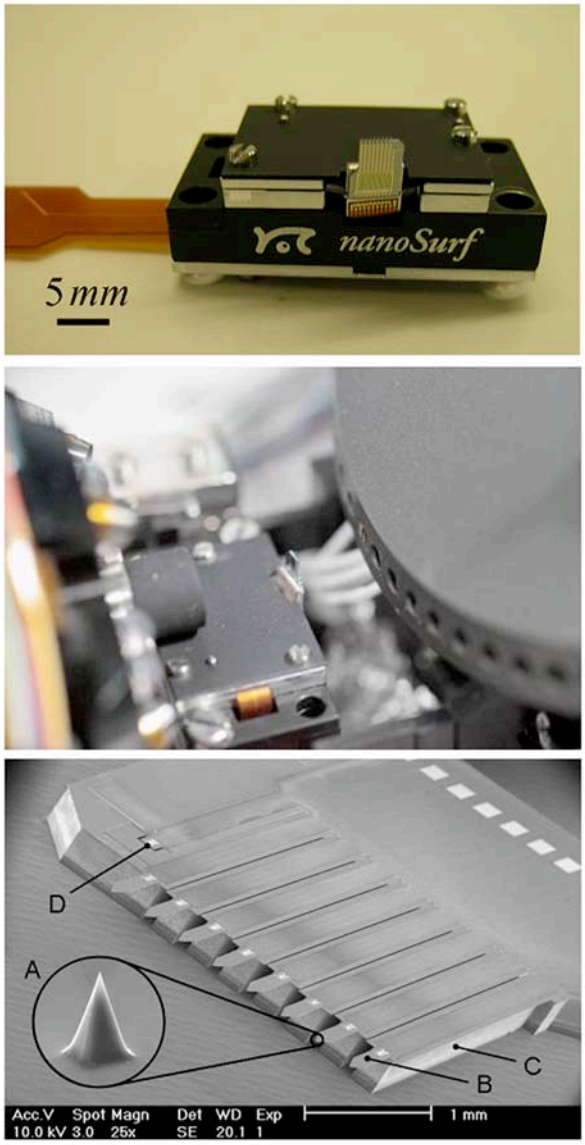

Figure 12. (top) The AFM scanner viewed from the perspective of the sample. (middle) The scanner positioned under the nose of the OM and in front of the SWTS. (bottom) The AFM chip. A notes a close-up of one of the silicone tips and B notes one of eght cantilevers mounted on a cleavable support-beam (which is noted by C). D notes a reference piezoresistor used for temperature compensation.

unit, featuring a 2.0 mm OD, 0.1 mm increment, and 7.5 μm line width, as well as an image of a square grid target used to detect aberrations such as pincushioning and barreling. No significant optical image distortion can be seen across the 1 $\times$ 2 mm field of view, and resolution of the 5.0 μm line suggests that the microscope resolution is limited by the pixel size. This conclusion was subsequently confirmed by characterizing an identical optical system with a higher resolution CCD.

[33] The depth of field of both the electron and fluorescence microscopes (EM and FM, respectively) were calibrated at the University of Arizona using a Ronchi grating tilted at 10:1 such that the edges are intentionally out of focus (Figure 7). A depth of field greater than 50 μm was measured by determining the extent of the in-focus region. This measurement also served to calibrate the best focus position and to confirm that the image plane is orthogonal to the OM axis.

[34] The linear response of the red, green, blue, and ultraviolet LEDs was determined from images of a broadband optically reflective white Spectralon® from Labsphere, Inc. (a broadband optically reflective target formed from Teflon spheres), polished for uniformity. The 12-bit counter saturates at 4095 counts, limiting the acceptable exposure. A measure of image acquisition speed with the UV LED was derived from measurements of the LED composite spectrum acquired using an Ocean Optics USB 2000 Spectrophotometer. The integration time was 200 ms for the visible LEDs and and 1 s for the UV LEDs. Figure 8 shows the physical arrangement of the LEDs.

[35] The OM focal plane array scheme is the same one used for the RAC [*Kramm et al.*, 1998]. Data are returned with 12 bits/pixel. Typical exposure times are 0.3 to 0.7 s., depending on the selection of LEDs that provide the illumination. In general, the illumination strategy will be keyed to typical particle reflectivity rather than the reflectivity of the various substrates. The target signal-to-noise ratio is 200:1 for 100 msec exposure.

[36] The spectral response of the optical and detector system was measured for the identical EM unit by filtering an integrated light source through an Acton SP-150 monochromator onto an integrating sphere, which was then calibrated by an Ocean Optics USB 2000 spectrometer (Figure 9). A series of full aperture images were acquired at over a 400–1000 nm range at 5 nm steps using a 5 nm bandpass. Each data point was derived from three live frames (512 $\times$ 256 $\times$ 12 bit), one dark frame using the same integration time, and a shutter frame (a single clock

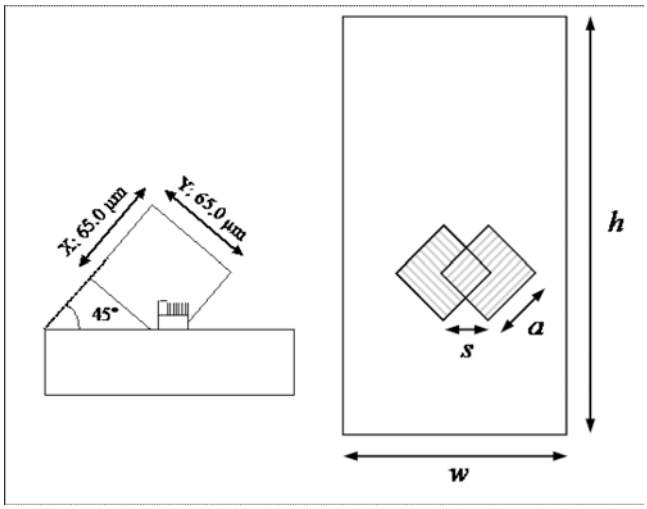

Figure 13. (left) Geometry of the AFM scan field relative to the OM coordinate system. (right) This exaggerated diagram shows the AFM scanning at 45° relative to the OM axis. The field can be shifted laterally (but not vertically) by rotating the SWTS in 15 μm increments (s). The actual OM image is 2 (h) $\times$ 1 (w) mm while the diamonds are 65 μm on a side (a), covering about 2.5% of the optical field.

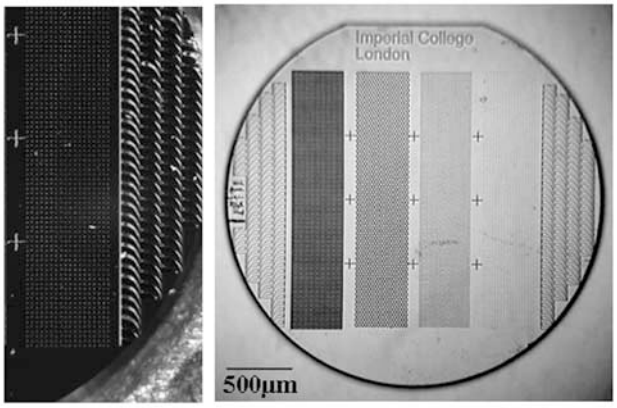

Figure 14. (left) OM test bed image of textured substrate, processed to appear like flight image. (right) Conventional microscope image showing full substrate.

cycle with illumination on). The dark frame and shutter frames were subtracted from the average of the live frames.

[37] A flat field correction for the optical and detector system was determined by pointing the OM into an integrating sphere illuminated as described above using wavelengths corresponding to the four LED colors (375, 466, 543, and 636 nm). Integration times were varied by increments of 10% relative to a value empirically determined to be near full-well but with no saturated pixels. Unilluminated images were similarly acquired as a background reference. In a separate measure of OM linear response, each of the twelve LEDs was individually focused on a flat Spectralon diffuser covered by a microscope slide (Figure 10). Images were then acquired as for the monochromator test.

[38] Figure 11 shows the composite output spectrum of the LEDs, measured with a spectrometer coupled to an integrating sphere with a fiber optic. In more extensive tests of LEDs from the same lot it was determined that the LEDs do not change their peak wavelength as they warm up, but the bandwidth widens slightly. The UV LED has a filter to insure no shift in wavelength.

6. Atomic Force Microscope

[39] As shown in Figure 1, the MECA AFM is located between the OM and the SWTS inside the darkened MECA enclosure on the spacecraft deck. It scans a small region (from 1 to 65 μm square) on any of the 69 substrates, each 3-mm in diameter, positioned along the rim of the SWTS. The chief scientific objective of the AFM is to analyze small dust and soil particles in terms of their size, size distribution, shape, and texture. The AFM is particularly well suited to analyze particles carried by the wind, which are believed to be in the size range 1–3 μm. Prior to AFM scanning, OM images are acquired to document the substrates and provide context for the AFM scans.

[40] The AFM is contributed by a Swiss-led consortium spearheaded by the University of Neuchâtel. Run by a dedicated microcontroller, the AFM uses one of an array of eight micromachined cantilevers with sharp tips to obtain topographs (sometimes called "scans" or "images") of up to a 65 $\times$ 65-μm area of the sample. Within this constraint the scan can be of any size, dimension, or orientation, but the AFM can only address a narrow horizontal stripe of each substrate. Since the sample wheel can be rotated (but not elevated) prior to initiation of scanning, the AFM can access a thin band approximately 1/3 of the way up from the bottom of the corresponding OM image.

[41] MECA's AFM comprises three major components, a microfabricated probe-chip, an electromagnetically actuated scanner, and single board control electronics. The probe-chip features 8 high aspect ratio silicon tips mounted on thin cantilevers, which are in turn mounted on sturdy silicon beams (Figure 12). A piezoelectric disk on the chip provides the excitation for the cantilever array [*Gautsch et al.*, 2002]. The chip is mounted with two orthogonal tilt angles of 10° relative to the sample to ensure that only one tip contacts the sample at a time. In case of contamination or malfunction of this front-most tip, the defective cantilever and its support beam can be cleaved off by a special tool on the sample wheel, after which the next one in the array becomes active. The array geometry is designed to spread the resonant frequencies of the levers between 30 and 40 kHz in order to avoid cross-talk during dynamic operation. The force constant of the levers varies between 9 and 13 N/m.

[42] Each of the 8 MECA cantilevers features an integrated piezoresistive stress sensor, which is used to measure its pure deflection (static mode) or its vibration amplitude, frequency and phase (dynamic mode) [*Akiyama et al.*, 2001]. The piezoresistors are addressed by a multiplexer, which links them to a temperature-compensated Wheatstone bridge. In static mode the deflection signal is proportional to

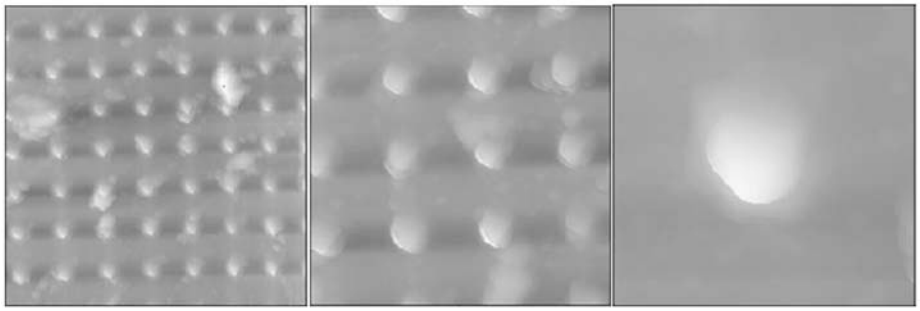

Figure 15. AFM images of pincushion target at various scales. Image sizes are (left) 15, (middle) 8, and (right) 2.4 μm and the corresponding gray scales span 2, 2.5, and 1.73 μm. Figure 15 (right) uses 9.4 nm per lateral step and the transition on and off the peak is nearly abrupt.

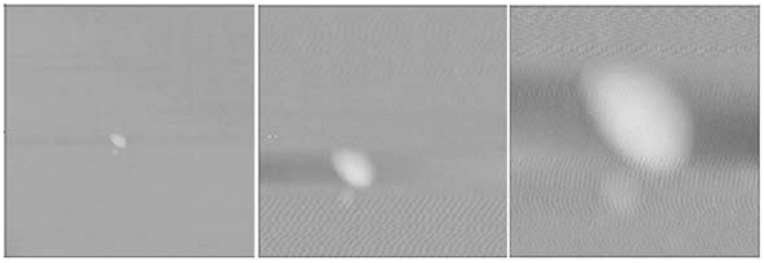

Figure 16. AFM image of a basalt particle at various resolutions. Image sizes are (left) 5.11, (middle) 2.04, and (right) 0.82 μm and the corresponding gray scales span 0.355, 0.205, and 0.14 μm. The transition from background to particle is about 5% of the lateral field or $\sim$40 nm.

the force, which the microprocessor holds constant at a designated setpoint by adjusting the distance to the sample. In dynamic mode the resonant frequency of the cantilever is excited by a phase locked loop and the shift of the resonance frequency provides a measure of the force gradient. The microprocessor holds the resonance frequency at a designated setpoint by changing the distance to the sample. Additionally the phase-shift changes between the excitation and the reaction of the cantilever can be measured. Dynamic mode minimizes the interactions between tip and surface and is less likely to result in particles being moved around or dislodged during the scan. In either mode, these signals are used to regulate the distance between the tip and the sample in the z-direction by means of a proportional-integral feedback loop. While the MECA AFM supports imaging in either mode, tests of Martian analog material indicate that the dynamic mode will be most useful for imaging dust particles without undue particle motion.

[43] Scanning is achieved using an electromagnetic actuator. Such an actuator does not require the high voltages of the more usual piezoelectric scanner and provides a large scan range of up to 65 μm for maximizing the resolution overlap between the OM and AFM. The z axis servo signal represents the sample topography as the tip is rastered across the surface in the x (fast) and y (slow) directions. Imperfect feedback or an out-of-range condition can result in residual bending of the cantilever in static mode, or a frequency shift of the oscillation in dynamic mode. This error signal is recorded in a second data channel. Since each line in the raster scan begins at the same point on the x axis, both primary and error signals are recorded on both the forward and the backward legs of the scan. Thus a single raster scan produces four arrays of data: Forward (signal), forward (error), backward (signal), and backward (error).

[44] It must be emphasized that an AFM scan is acquired by rastering a physical tool across a surface. As a result, line-to-line noise and artifacts may be significantly different than point-to-point artifacts along the scan direction. Moreover, outside the range of authority of the cantilever (approximately 65 $\times$ 65 μm laterally and up to 13 μm in height) the topograph does not go ''out of focus'' but simply saturates, while anywhere within its range of authority it is equally ''in focus.'' The topograph itself reflects the interaction between a tip of finite size and a nonuniform surface, and therefore convolves physical characteristics of both the probe and the target. Thus, while an AFM topograph may look like an image product, the processing required bears little in common with the processing of an actual optical image.

[45] Two challenges of using an AFM to study Martian soils deserve special mention. The first is the challenge of using the technique to study loose, irregularly shaped particles. The second is the general challenge of operating an AFM autonomously, particularly without the ability to exchange used, damaged, or contaminated tips. On Earth, the AFM is seldom the technique of choice for the study of particles, as a Scanning Electron Microscope (SEM) is more versatile with respect to high-aspect-ratio, loosely bound material. The AFM tends to detach particles and push them around, and unlike the SEM, it cannot view irregular surfaces from different angles. While the AFM is the pragmatic choice for Mars and other space applications, there is little in the literature to offer guidance on methodology and performance of AFMs with respect to particulate samples. Kempe et al., for example, glued sand grains to a macroscopic substrate prior to investigating them [*Kempe et al.*, 2004]. This approach is, however, not practical for a planetary mission. Indeed, much of what is known relevant to the Phoenix SWTS has resulted from investigations with this particular instrument [*Gautsch et al.*, 2002; *Marshall et al.*, 2001; *Vijendran et al.*, 2007].

[46] Even in dynamic mode, particles can become a contamination hazard to AFM tips when they adhere more strongly to the tip than to the substrate. Such particle adhesion can degrade the scans in question and the quality of the tip in general. Several design decisions were made to

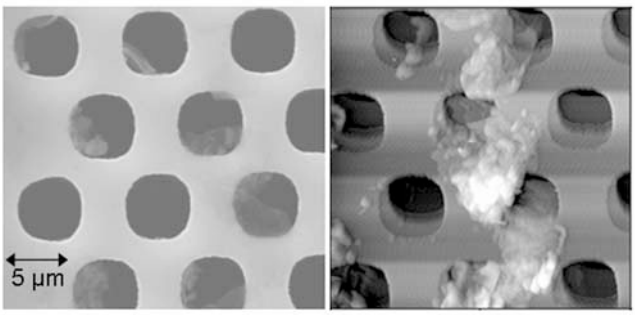

Figure 17. (left) SEM and (right) AFM of textured substrate. It is possible to distinguish $\sim$50 nm vertical resolution out of $\sim$500 nm vertical range. The AFM image was acquired on a commercial Nanosurf system.

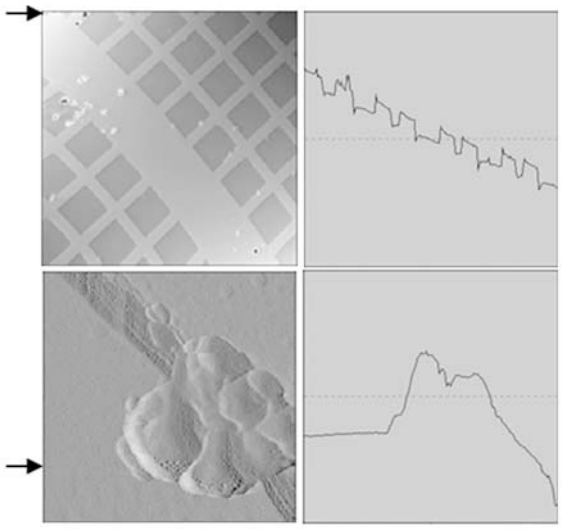

Figure 18. (top left) Linear grid, 10 μm pitch, imaged by MECA AFM (stand-alone system). The image is 52.9 μm wide, 256 $\times$ 256, with 207 nm per step. The vertical step size is 14 nm. (top right) A cross section through the same image with 3.46 μm vertical scale, showing an abrupt step at the grid transitions laterally and noise of a few steps vertically. (bottom left) Derivative rendering of 2 μm wide, 256 $\times$ 256 MECA AFM image of contaminant particle from grid. A lateral step is 8.1 nm. (bottom right) Cross section through the corresponding raw image with 0.86 μm vertical scale, 3.4 nm per vertical step. The transition at the left edge of the particle is $\sim$70 nm wide.

mitigate this threat. The vertical imaging orientation of the SWTS substrates was chosen as a simple way to produce a sparse field of particles, but it also ensures that retained particles are modestly well bonded to the substrates. Of the six substrates in each set, two are specifically designed for AFM use in that they resist the tendency for particles to become dislodged and to adhere to the AFM tip. One of these substrates is a uniform piece of silicone that remains pliant under Martian conditions. The second is a custom micro-machined silicon substrate with pits and posts that hold particles of an appropriate scale for AFM scanning. Two of the remaining four substrates are magnets that may, under certain circumstances, be appropriate for AFM scanning. The final two substrates are deep ''buckets'' that would not normally be accessible to the AFM.

[47] While the MECA AFM is capable of addressing areas up to 65 μm on a side in up to 512 $\times$ 512 pixels, the typical topographic height in such a large area would exceed the vertical range of the MECA AFM scanner ($\sim$13 μm), and we therefore expect to acquire scans with 10–30 μm on a side, typically contained in 256 $\times$ 256 pixels for a lateral granularity of $\sim$0.1 μm/pixel. This is still a relatively coarse size regime for an AFM, and as a result the scanner is relatively insensitive to environmental conditions such as vibration and thermal gradients.

[48] Recognizing both the virtue of simplicity and the limited time and bandwidth for AFM scanning, the MECA SWTS was not built with a mechanism to translate the substrates vertically with respect to the imaging axis. As a result, the AFM can only access an $\sim$0.1 mm horizontal band within the 2 mm high by 1 mm wide sample area imaged by the OM, centered approximately 0.7 mm above the bottom of the OM image. As shown in Figure 13, the x and y axes of the MECA AFM image are rotated by +45° relative to the OM images.

[49] Figure 14 shows the 2 $\times$ 1 mm OM field of view, as determined by the spacing of the features (see adjacent mask reference). The SWTS rotational step size is 15 μm. All necessary AFM calibration can be performed in situ without need for external equipment, using three calibration substrates. A regularly spaced precision grid is used to establish the relationship between the commanded coordinates and actual coordinates, correcting for the characteristic saddle distortion and shrinkage of the overall scan range as temperatures are lowered. Even with a prior laboratory calibration, the actual sample temperature will not be known, and significant variation will also result from small temperature gradients or slow temperature drift. As a result, frequent in situ calibration is the only reliable method of correcting images to compensate for instrument artifacts such as saddle distortion.

[50] A second pincushion calibration grid is used to determine the shape of the AFM tip itself. An AFM image is a dilation of the shape of the substrate and the tip shape, a property that can change as tips become contaminated with

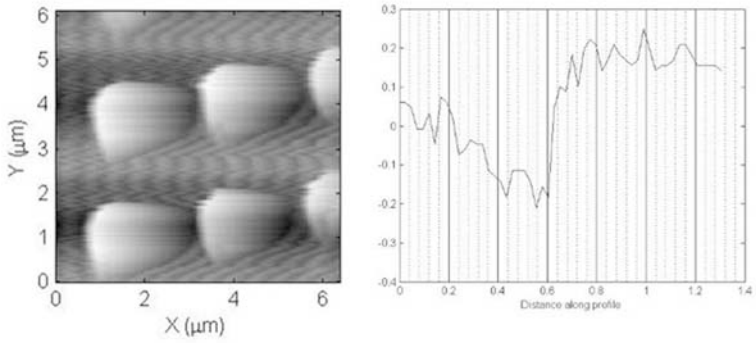

Figure 19. (left) Pincushion calibration grid imaged with Imperial College Test bed system. (right) Profile along the y axis through a grid element. The minor gridlines are 0.4 μm.

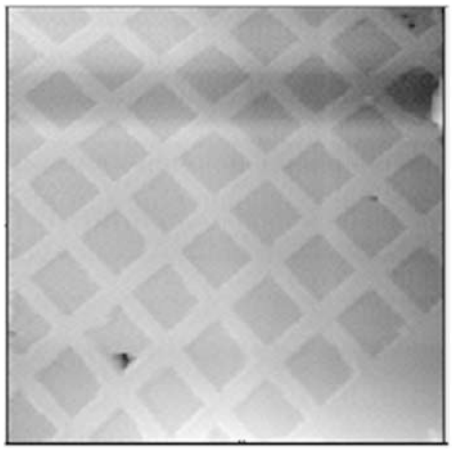

Figure 20. AFM image of calibration target (line spacing 10 μm) demonstrating 65 μm range of scanner. The images were acquired on the FM scanner in testing prior to shipment to JPL.

dust or become dull due to micro-fracture and wear. Moreover, only the first of the eight available tips can be calibrated prior to its use, so the tip shape can only be determined when the previous beam is broken off. Thus, like the distortion correction, tip shape must be determined regularly in situ.

[51] A third calibration substrate, the tip finder, is used to associate each AFM tip position with the corresponding optical microscope field, making it possible to use the AFM to obtain a high resolution image of a structure of interest. Using silicon microfabrication techniques, the tip-finder is encoded with unique raised structures on a micron scale such that an AFM image of any portion is unique and recognizable. Since the AFM tip array has a precise, fixed shape, in situ use of the tip-finder should not provide any new information. It has been included in the calibration suite in the unlikely event that macroscopic translations occur due to vibration or mechanical failure of the AFM sample train. A final aspect of the calibration is determination of the unique resonant frequency used to identify each AFM tip. The frequency of the active cantilever is measured each time the AFM is initialized.

[52] AFM resolution is conventionally interpreted as a property of the scanner, since the actual resolution of a topograph is a combination of the tip condition, the nature of the sample, the sample mounting, and environmental factors. Moreover, while it is empirically useful to determine the smallest resolvable features for a particular class of substrates, this property must be inferred from natural features because of the lack of manufactured standards in the nanometer size range. We have, nonetheless, analyzed a number of samples of discrete structures in order to characterize the resolving capability of the MECA AFM.

[53] Figure 15 is a series of AFM images of the pincushion target acquired at the University of Neuchâtel on a system that uses the same scanner and electronics as the MECA FM but a different sample stage. The highest magnification image is ~10 nm per step and the transition on/off the sharp peak is nearly abrupt. Figure 16 is a similar zoom series of a rounded particle, acquired on the same system. In this case the transition at the edge of the particle is ~40 nm wide. It can be concluded from these images that the scanner can laterally resolve features finer than 50 nm.

[54] Figure 17 compares SEM and AFM images of one of the textured substrates fabricated by Imperial College and used in each sample set on the FM SWTS. In this rendering the depth is color-encoded, and sharp definition can be resolved between features spanning ~5% of the full color range, or 25 nm. Figure 18 shows cross sections through images of a 10 μm pitch linear grid with 14 nm and 3.4 nm per vertical step, respectively. In each case features can be discerned over a few vertical steps. Figure 19 shows a cross section of an abrupt feature from an image of the "pincushion" calibration grid of the type that will fly on Phoenix. This image was acquired on a test bed at Imperial College with flight-like SWTS and AFM. It can be see the high-low transition occurs in ~0.08 μm lateral distance. It can be concluded from these images that the scanner can vertically resolve features finer than 25 nm.

[55] The lateral range of the AFM at room temperature was determined empirically to be 65 μm square by scanning a standard calibration target (Multifunction Target $4x-20x$ from Max Levy Autograph, Inc.) with a 10 μm spacing

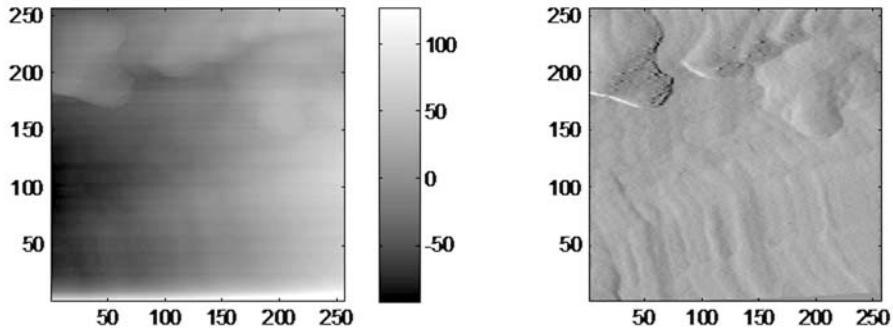

Figure 21. AFM scans (256 × 256) of a section of the anodized aluminum sample wheel, acquired at the Payload Interoperability Test bed on 7 December 2006, using channel gain 2 (vertical step size 12 nm) to bring out finer features. The scan is of a field 10 μm on a side acquired at a speed of 3.5 s/line. (left) The raw topography, and (right) line-by-line derivative, which better simulates what the eye would see if this were a macroscopic, illuminated surface.

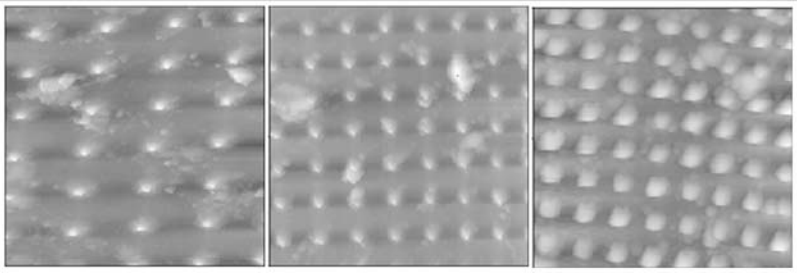

Figure 22. AFM image of pincushion with tip 4 for (left) scan 1 (10.1 μm square), (middle) scan 30 (15.1 μm square), and (right) scan 80 (15.1 μm square). Gray scales span 1.5 μm (Figure 22 (left)), 2.0 μm (Figure 22 (middle)), and 2.5 μm (Figure 22 (right)).

(Figure 20). The AFM spans the full range of topography ($\sim$12 μm) in the vertical direction by encoding a fraction of that range in 8 bits, or 256 levels. The fraction is set by a commandable channel gain such that 0 spans the entire range and each subsequent increment reduces that range by a factor of two. Thus the maximum channel gain setting of 8 restricts each line scan to 1/256 of the available 12 μm, or 47 nm (the centroid is adjusted after each line). That range is spread across 8 bits (256 levels) such that 1 DN corresponds to 0.18 nm, allowing a factor of 5 margin for drift and calibration changes. As an example of the influence of the gain setting, Figure 21 compares two images of the same region using gain settings 0 and 2. In Figure 21, channel gain of 2 (vertical step size 12 nm) brings out the fine texture of the relatively flat anodized aluminum. In practice, it is not expected that gains higher than 2 will be utilized during the mission.

[56] Tip wear was studied by repeated imaging of the pincushion array. Figure 22 shows the gradual degradation of AFM scans at various stages, and Figure 23 shows the worn tip itself as imaged by a scanning electron microscope after 90 scans.

[57] Finally, Figure 24 demonstrates the ability to target a feature with the AFM that was identified in a previous OM image, limited only by the 15 μm rotational step size of the SWTS.

7. Sample Wheel and Translation Stage

[58] The two-degree-of-freedom SWTS rotates to select a set of substrates for sample deposition or a portion of a single substrate for imaging. It translates to position the sample wheel outside the MECA enclosure to accept soil specimens from the robotic arm, to remove excess dirt by dragging the sample a metered distance under a blade, to focus the substrates for imaging, and to effect a coarse approach to the AFM. The SWTS is moved by a pair of stepping motors such that, in the absence of slipping, a simple count of the commanded steps determines the position. Dual limit switches are incorporated into the sample wheel rotation and the stage translation to prevent overdriving, to indicate the position at the ends of the translation sequence, and to indicate a reference position for the wheel. The SWTS fits within a 16 cm long by 12 cm wide by 12 cm tall envelope, including the AFM mount. It weighs just over 1 kg.

[59] The SWTS must have sufficient mechanical and thermal stability to allow reproducible high resolution imaging and to retain the substrates and calibration standards such that their front surfaces are in a well-defined position relative to the microscope. It must allow for substrate illumination, mounting, and alignment to both the AFM and the optical microscope. It is designed to minimize cross-contamination of substrates and to protect delicate portions of the instrument until it is deployed on the surface of Mars.

[60] In the following discussion a "sample" refers to a specimen of Martian soil, while a "substrate" refers to the base or platen on which the samples are deposited. The arrangement of the substrates on the wheel is shown in Figure 3. The 69 substrates are divided into ten sets of six, each of which can be exposed for soil delivery as shown in Figure 1, and nine utility or calibration targets. Of the six substrates in each set, one is a uniform piece of silicone that remains pliant under Martian conditions. The second is a custom micro-machined silicon substrate with posts and pits ("nanobuckets") that hold particles of an appropriate scale for AFM scanning. Two of the remaining four substrates are weak and strong magnets. The final two substrates are single microbuckets 3 mm in diameter and more than 2 mm deep, designed for OM imaging of bulk-like samples. Except for the microbuckets, each substrate has an exposed diameter of 3 mm with 4.1 mm bases such that they can be flush mounted from behind the 3 mm opening.

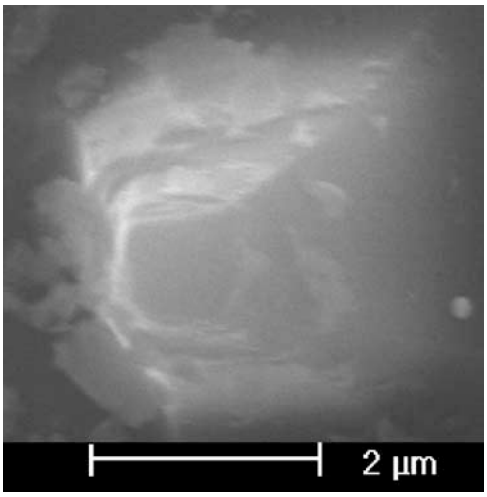

Figure 23. SEM image of tip 4 after 90 scans showing debris and minor blunting.

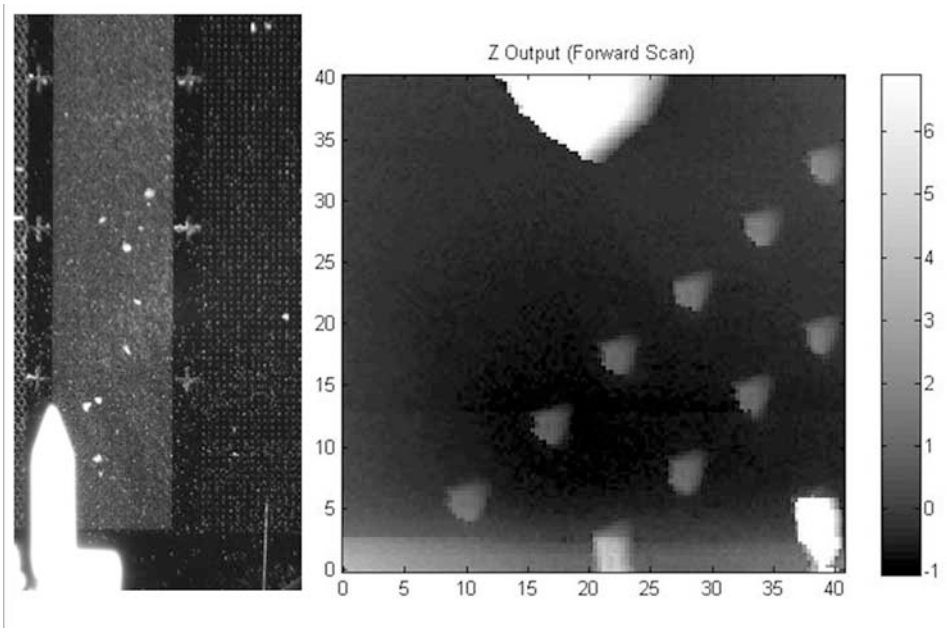

Figure 24. (left) OM image targeting the edge of a strip of 3 μm pillars. (right) AFM image showing the onset of the targeted strip (note that the AFM image coordinates are rotated 45° relative to the OM). Dimensions are in μm.

[61] To acquire samples, the wheel moves in and out of an opening in the end panel of the enclosure when the sample wheel translates. With the exception of magnetic substrates, the shape of the opening and additional baffling resists contamination of clean substrates by spilling of particles from adjacent substrates (Figure 4). A notch in the sample wheel is placed in front of the microscope in the stowed configuration to protect the AFM from vibration or shock-induced translation of the stage prior to operation on Mars (Figure 25). Each substrate position on the sample wheel is identified by laser-etched numbering, as seen in Figure 26.

[62] For translation of the SWTS, extension, or "outward," is defined as the direction that moves the sample wheel out of the box for sample delivery. Retraction, or "inward" moves the sample toward the microscope. From the point at which the wheel touches the inside edge of the enclosure, an extension of 5 mm completely exposes the substrates after passing them under the leveling/scraping blade mounted on the enclosure. Retraction of just under 1 cm from the fully extended position brings the substrates back inside the box to the focal position. A coupon table in the software records the optimal focus position for each substrate, which varies slightly from substrate to substrate due to runout on the wheel surface (±0.1 mm).

[63] The range of commandable focus positions allows for the maximum height of any particle on the substrate. The leveling blade, which rides slightly above the surface of the wheel, is designed to limit the particle size to 0.2 mm, with 0.025 mm tolerance in the alignment of the substrate surfaces to the wheel surface. With the exception of magnetic substrates, which scavenge loose particles, this strategy limits the sample particles to project no more than 0.2 mm above the nominal front surface position of the substrates. On the strong magnet, piles nearly 1 mm high have been observed. Figure 27 shows such a pile on a weak magnet substrate, imaged at Imperial College with the OM in a through-focus series.

[64] The rotational step size of the wheel at the surface of the substrate is 15 μm, reproducible to within an OM pixel (4 μm) as determined by comparing OM images shifted by a

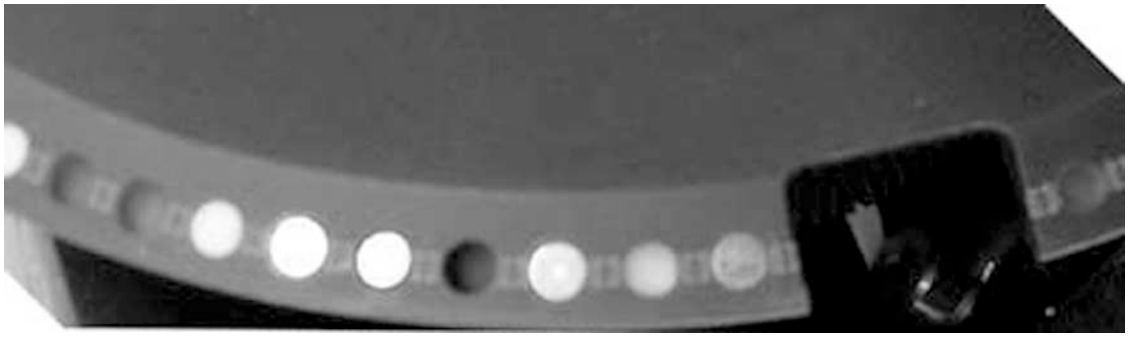

Figure 25. Sample wheel notch (shown on right). Note that substrate arrangement shown here is not the same as on the flight unit.

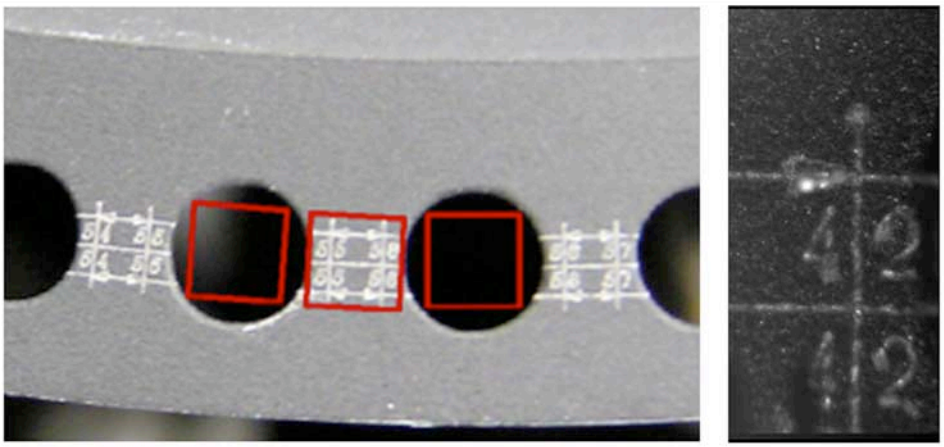

Figure 26. (left) Sample wheel numbering (from external camera). (right) Sample wheel numbering (with OM).

known number of steps. The translational step size of the FM SWTS is 0.25 μm, routinely reproduced to within a few steps as confirmed by measurement of the macroscopic separation of the limit switches. The fine step size is required in order to place the AFM tip near the center of its $\sim$12 micron vertical range (i.e., normal to the sample, parallel to the translation direction) when it comes in contact with the surface. This is accomplished by moving the sample wheel forward in 0.25 μm steps and stopping on a signal from the AFM. The smooth, fine translational motion is achieved in large measure by the use of flexures that link the fixed and translating part of the wheel. As an artifact of the flexures the substrates dip downward at the extremes of motion relative to the microscopes. In particular, the substrates will drop approximately 100 μm from the OM focus position to the AFM scan position, a useful characteristic because it prevents the region accessible to the AFM from being obscured by the cantilever in the OM image.

[65] The SWTS was modified from the heritage 2001 design to include a finger that damps out jitter or vibration, eliminating the need to maintain any holding torque (Figure 2). Lubrication and shielding of bearings and critical components was designed to make the SWTS resistant to dust contamination. Laboratory calibration of the SWTS consisted of confirming the relationship between stepping motor steps and distance traveled (rotation and translation); precisely determining the position of each limit switch; measuring backlash; and mapping the precise position of each substrate, including the cleaving tool, both in translation and rotation. A stray-light test was performed using the MECA OM test bed with overhead illumination from a laminar flow bench. Images were acquired of red, white, and UV calibration targets in 5 different illumination configurations; RGB, R, G, B, and none. Images were acquired with and without the enclosure.

[66] The darkened enclosure is not intended to be entirely light-tight, as cables need to enter and exit and soil must be introduced to the wheel, but it must reduce background light sufficiently to allow the LED illumination to dominate. The rightmost points in Figure 28 compare the measured intensity of a 1-s image with and without the cover. A ratio of 5600:1 was observed. It can also be seen that with the LEDs

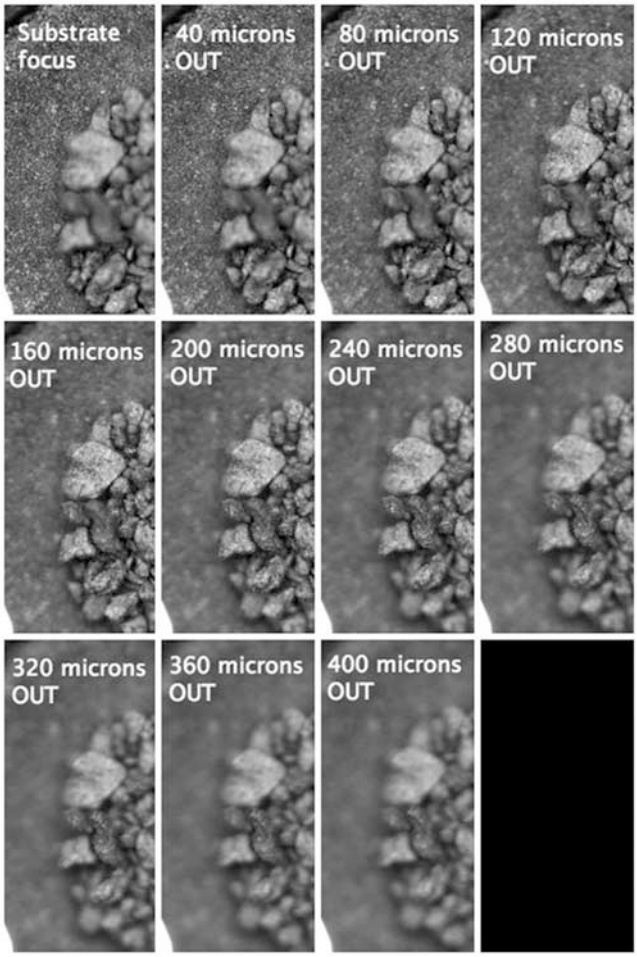

Figure 27. A through focus series of OM images of the strong magnet. Images focus at progressively higher planes, with the first image (upper left) focusing just above the substrate and the last image (lower right) focusing at the top of the highest particle.

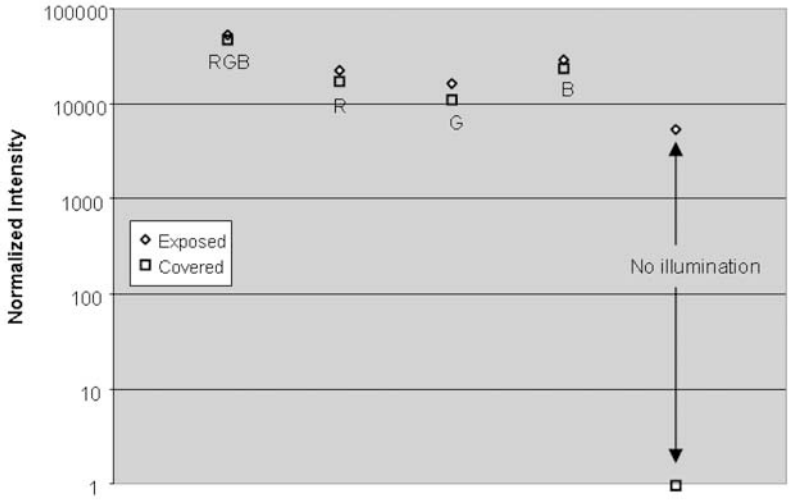

Figure 28. Measurements of a red target with and without cover.

on, removing the cover makes little difference in the intensity, suggesting that stray light does not significantly affect the images even with the cover off.

[67] Table 1 summarizes the nine special substrates included to (1) determine linearity and magnification of the AFM and optical microscope, (2) calibrate colors for the optical microscope, (3) register the AFM image to the OM image, (4) clean AFM tips, and (5) break off used beams from the tip array.

[68] The UV calibration target is a tablet of $BaMgAl_{10}O_{17}$:Eu^{2+} (BAM) prepared by *Zych et al.* [2004] using a process of pressing and sintering at 1750°C for 15 h. Photophysical properties are very similar to the pre-sintered powder and to the commercial powder (available, for example, from Philips Lighting Inc.). BAM absorbs in the entire UV (220–440 nm) and has a comparatively flat excitation spectrum, especially in the spectral region 250–350 nm as shown in Figure 29. The decrease in excitation strength at wavelengths shorter than 250 nm is likely an artifact of the low intensity of the incoming radiation. Emission is from the Eu^{2+} ions by the decay process $4f^6 5d \rightarrow 8S_{7/2}(4f^7)$ and appears as a single broad peak centered at ~450 nm, as shown in Figure 29a. The decay time constant is approximately 1100 ns. The quantum efficiency is greater than 50% and thus more than half of the incident UV photons are reemitted as blue-green photons. Figure 29 also shows the relative response of the UV target to illumination at a wavelength similar to that of the UV LED (images with the actual UV LEDs are essentially the same). Absolute quantum efficiency, expected to be around 80%, is difficult to measure, so the image has been normalized to unity. Also note that the flight tablet has an irregular shape. This defect does not affect the performance of the material and helps align images of the mounted target to the pre-flight luminescence maps.

[69] OM Calibration targets include a flat white painted surface provided by the University of Arizona for calibration of LEDS that have a temperature dependent radiant output; a ''stitching'' target consisting of microtext to be used to assess the parameters for joining mosaics of adjacent images; and a standard linear calibration target with lines, circles, squares, bars, and numbers (Figure 30).

[70] The Tip Finder is a coded substrate designed by Surface/Interface, Inc. to have distinct features that allow registration on both the OM and the AFM scale. This will be used to register the AFM tip positions to the OM image, a critical step in AFM target selection. An AFM image of this target using a flight-like MECA test bed is shown in Figure 31.

[71] On the left in Figure 32 is an SEM image of the AFM linear calibration standard, which is represented by the manufacturer (NT-MDT) to have a pitch of 3 ± 0.05 μm and an edge curvature radius of less than 10 nm. This will be used to correct for the large saddle distortion typical of

Table 1. Calibration Substrates and Tools

Substrate Type	Description
OM UV calibration	$BaMgAl_{10}O_{17}$:Eu^{2+} (BAM)
OM white calibration	White substrate for color LED calibrations
OM linear calibration	Standard optical target
OM stitching alignment	Text on silicon
Tip finder tool	Coded at AFM and optical scales
AFM tip breaking	Raised bar adjacent to relieved channel
AFM tip cleaning	Same as silicone substrates
AFM linear calibration	TGX1 for both AFM linearity and magnification; see http://www.ntmdt-tips.com/catalog/gratings/afm_cal/products/TGX1.html
AFM tip standard	TGT1 pincushion for determining AFM tip shape; See http://www.ntmdt-tips.com/catalog/gratings/afm_cal/products/TGT1.html

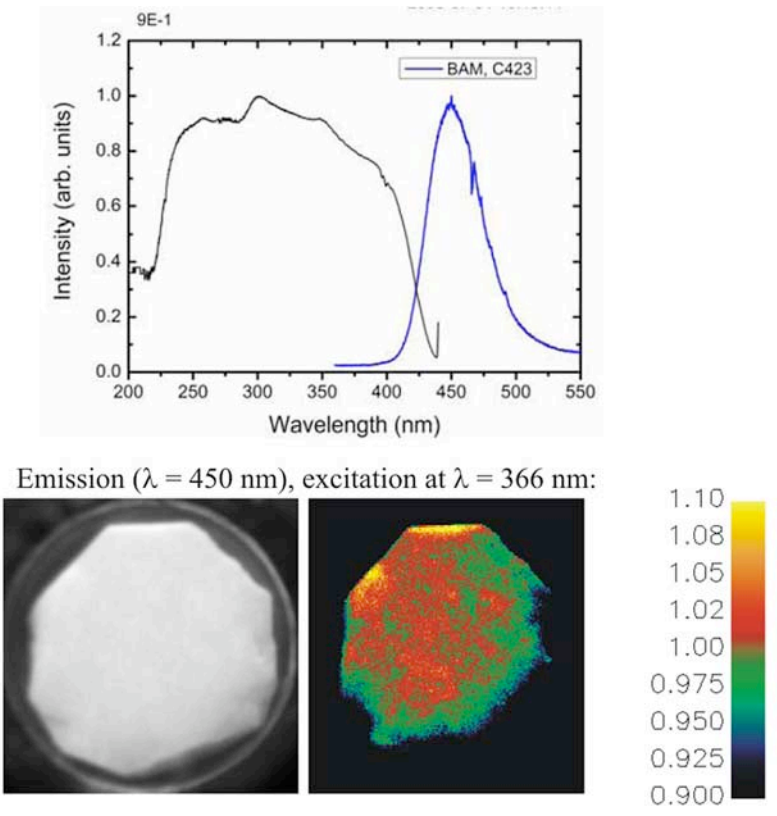

Figure 29. (top) Excitation (curve on left) and emission (curve on right) spectra of flight-like BAM tablets (batch C423). (bottom) UV luminescence map of the response of the flight UV calibration target to illumination by UV radiation at 366 nm. The color contour plots in are all normalized to unity, but the scale is proportional to the quantum efficiency of the luminescent tablet.

this type of AFM drive, and to establish an absolute length scale, which is expected to be a weak function of temperature (the scan size is reduced by 30% at −30°C relative to the size at room temperature).

[72] On the right in Figure 32 is an SEM image of the AFM Tip Standard (pincushion) calibration substrate from the same vendor, consisting of an array of extremely sharp tips with 2.12 μm pitch (3.0 μm across the diagonal), 0.3 to 0.6 μm height, and curvature of less than 10 nm. Since these tips have a higher aspect ratio than the AFM tip itself, it will be used to characterize the AFM tip shape.

[73] The tip-breaking tool is a prominent bar extending slightly above the surface of the sample wheel and placed adjacent to a small notch. The SWTS is moved toward the AFM, overriding the limit switch failsafe, until the bar contacts the beam and forces it backward. The notch accommodates the backlash of the remainder of the chip when the beam snaps off.

[74] The tip-cleaning tool is simply an additional silicone substrate. A short scan of this substrate has been shown to remove loose particles from the AFM tip.

8. Performance

[75] Prior to integration of MECA, calibration of the microscopy system encompassed referencing of substrate positions, detailed laboratory calibration of the optical and electronic properties of the optical microscope, similar calibration of the linearity and tip characteristics of the AFM, and determination of the relative position of AFM tips and the optical microscope field. The important properties of both microscopes will be determined in situ (both on Earth and Mars) using calibration targets mounted on the sample wheel.

[76] Characterization of the microscope system itself and its response to analog samples is being carried out using flight-like test beds by team members at the SETI Institute, Jet Propulsion Laboratory (JPL), and Imperial College of London. Each OM and SWTS is integrated with a base plate, enclosure, and sampling chute of similar construction to the flight unit. The SWTSs are of the same form, fit, and function as the flight unit. They differ only in minor details such as lubricants and fasteners. Two of the units (at JPL and Imperial College) also incorporate an AFM and its control board (mounted separately). Though the electronics use some different parts, the AFM and electronics are functionally identical to the flight units but will be operated by direct PC control via serial line using the vendor's "EasyScan" software. Separate control boxes provide PC interfaces for the OM camera, OM lamps, and SWTS motors and limit switches. Labview-based software is used for the control functions. Optics, lamps, and structures in the OM test beds are also flight-like, but the focal plane imager is a commercial Redlake unit chosen for the similarity of its response to the flight imagers. The intrinsic resolution of the Redlake camera is higher than that of the

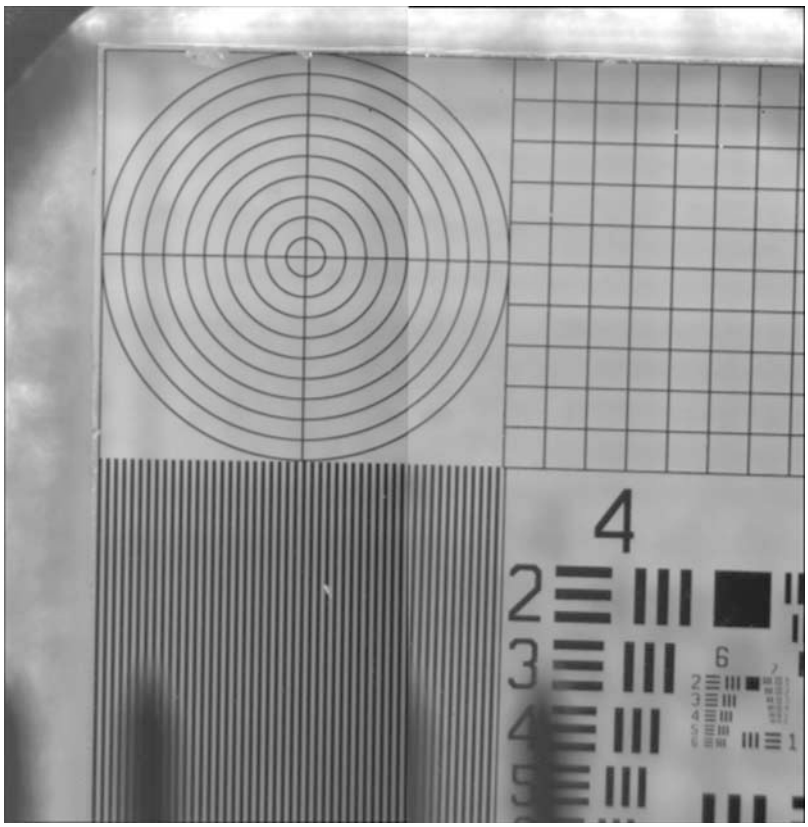

Figure 30. A mosaic of two adjacent images of the OM linear calibration substrate acquired with red LED illumination.

flight unit and its field of view is twice as wide; software is used to bin and crop the image to simulate the flight response. The full field, high resolution mode is used to determine the intrinsic resolution of the optics, and to monitor several of the AFM cantilevers that would be masked in the flight.

[77] The characterization investigations address the overall ability of the microscope to determine grain size, shape, color, texture, and magnetic properties as well as specific issues such as the amount of material retained by the different types of substrates and the manner of its distribution, the ability to recognize aggregates of particles or

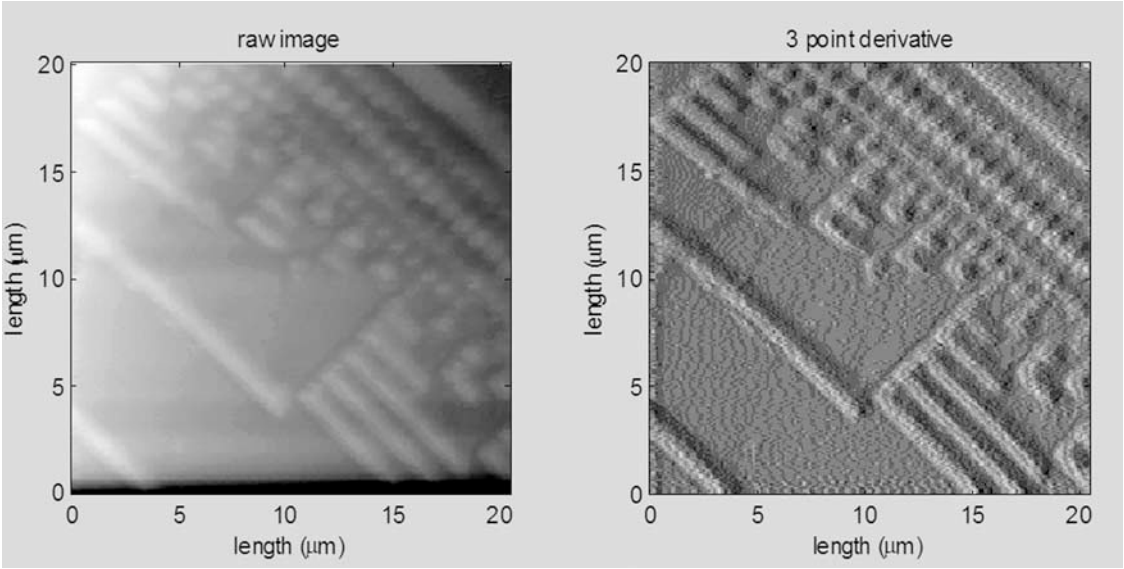

Figure 31. The 20 × 20 μm AFM scan of the tip finder substrate using channel gain 1 (corresponding to a 6.9 μm vertical range).

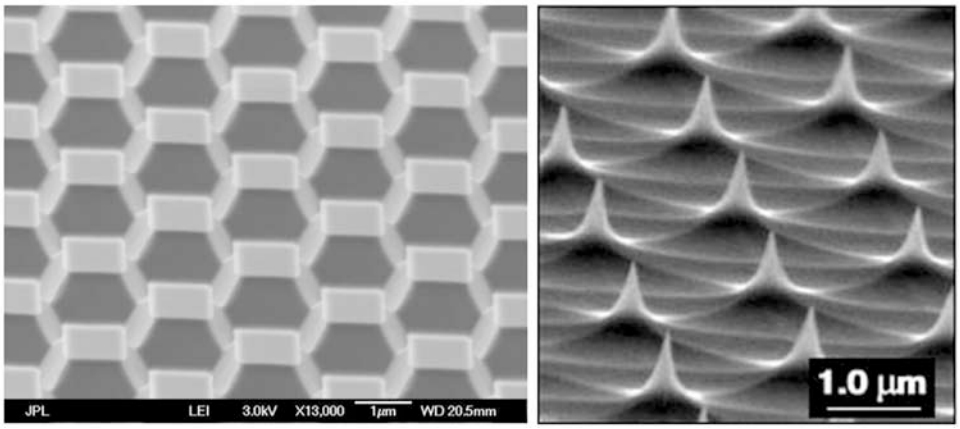

Figure 32. (left) SEM image of AFM linear calibration target. (right) SEM image of AFM tip standard (pincushion). Both are commercial products from NT-MTD.

parasitic attachment of small grains to large ones, and techniques to combine information from AFM and OM images. Also under investigation are aspects of sample delivery, including cross-contamination from previous samples, transfer of material between substrates, and the stability of the samples with respect to SWTS movement.

[78] The Microscopy Station will be used to analyze the size and shape of particles that are too small to be analyzed in the scoop by the Robotic Arm Camera (RAC). For larger particles (>100 μm) the RAC is preferable because the sample distribution in the scoop is more representative of the original distribution of material excavated by the robotic arm. For smaller particles, 1–100 μm in diameter, gravity is less important and the size distribution on the SWTS should be reasonably representative of the original. Here we define ''shape'' as grain surface curvature resolved in two dimensions, typically requiring measurement precision at least 10 times finer than the diameter of a grain.

[79] Particles of various size and shape were analyzed with the test beds as described above. AFM analysis at the University of Neuchâtel was performed using a scanner and electronics identical to the flight unit, but a sample stage of a different design. The smallest particles studied were 0.45 μm spheres, imaged with AFM at the University of Neuchâtel. The resulting topograph shown in Figure 33 (left) was recorded using 1 μm spheres and shows a rounded shape with some lateral distortion, which would normally be corrected using the transfer function determined from the linear calibration grid. A cross section (right) shows a rounded surface in the vertical direction.

[80] Size distribution assessment by manual AFM image analysis has been tested over the range that can be validated with a laser scattering method (Figure 34). The AFM counting technique results in good agreement, though the distribution is slightly sharper than the one determined with the laser method (it is unclear which is more reliable). The method can readily be extended to a higher resolution AFM field.

[81] Slightly larger particles, at the lower limit of resolution of the OM (4 μm/pixel), were evaluated using a sample of loose powder glass microbeads (3–10 μm) scattered on a nanobucket substrate. In Figure 35 the same particle is shown in an OM and an SEM image. The OM image indicates that the target particle is smaller than 8 μm

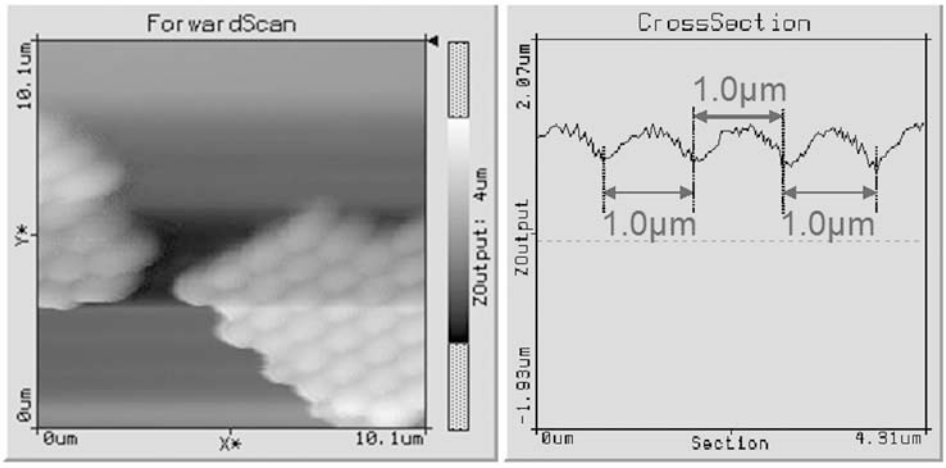

Figure 33. AFM image of 1 μm spheres and cross section indicating rounded surface profile with correct spacing.

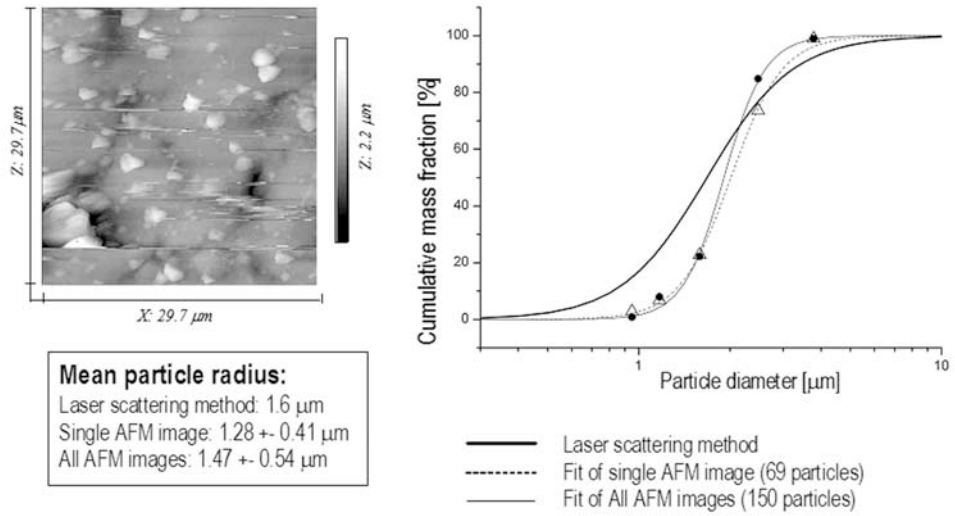

Figure 34. Determination of particle distribution with MECA AFM at University of Neuchâtel.

(2 pixels) in diameter. The SEM shows the particle to be approximately 6 μm in diameter.

[82] Shape discrimination was first studied using ballotini in the size ranges 10–53 μm and 44–74 μm. The ballotini was retained on all substrates to some degree, but best on magnets, even though the beads are nominally non-magnetic. Figure 36 shows conventional high-resolution microscopy images of the ballotini as well as the results from the MECA test bed optical microscope. The images clearly show that even the smallest particles are spherical in shape.

[83] Size distribution is in the process of being formally studied with the OM, but certain conclusions can be inferred from the images in Figure 36. In the leftmost image, the largest visible bead is ~56 μm (right in the middle of the pile). This corresponds within measurement error to the maximum size of 53 μm supposed to be in the distribution. No detailed count was done for smaller sizes, but it is reasonable to assume that they are at least as well retained as the larger particles. While the right hand image does not indicate particles as large as 74 μm, larger particles have been observed in other distributions, particularly in microbuckets. It can be concluded that in at least some cases, particles up to 100 μm are retained by the substrates such that they can be imaged. To the extent that particle loss is due to the competition between gravitation forces and van der Waals forces, on Mars the electrostatic attraction is expected to be much greater while the gravitational attraction is only 38% that on Earth. Consequently retention over most if not all of the desired range is likely. On the suspect larger end of the range, comparison with RAC images should allow skewing of the distribution to be detected.

[84] Angular grains were studied using an unsorted sample of crushed turbidite mudstone, with grains ranging from micron to millimeter size. This unwashed sample is one possible analog of the sort of material that will be found at our landing site – both the mixture of fines with coarser grains, and a subtle irregularity to particle shape rather than sharp shards. Imaging conditions were the same as for the ballotini, though the material was not retained on the substrates as well as the ballotini. Figure 37 shows a conventional high-resolution microscopy image adjacent to an OM test bed image. Although it would be hard to

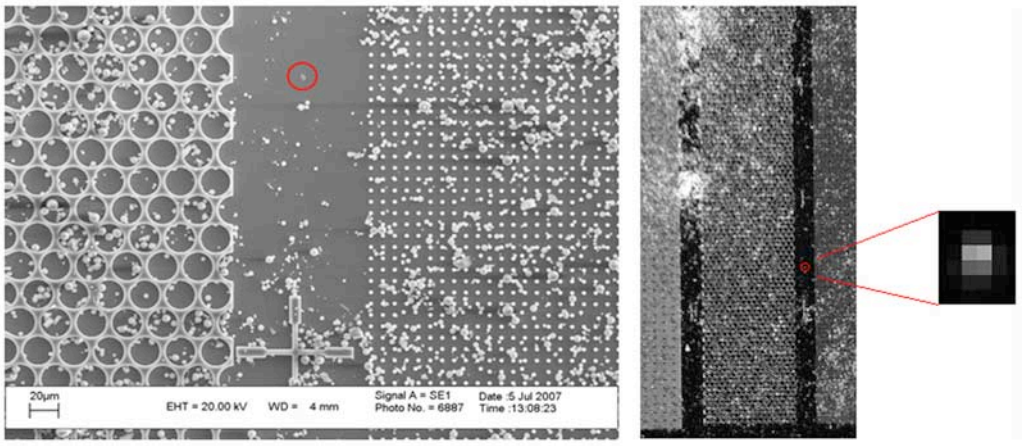

Figure 35. (left) SEM of a 6 μm particle. (right) OM image of the same particle with enlargement showing the individual pixel gray levels.

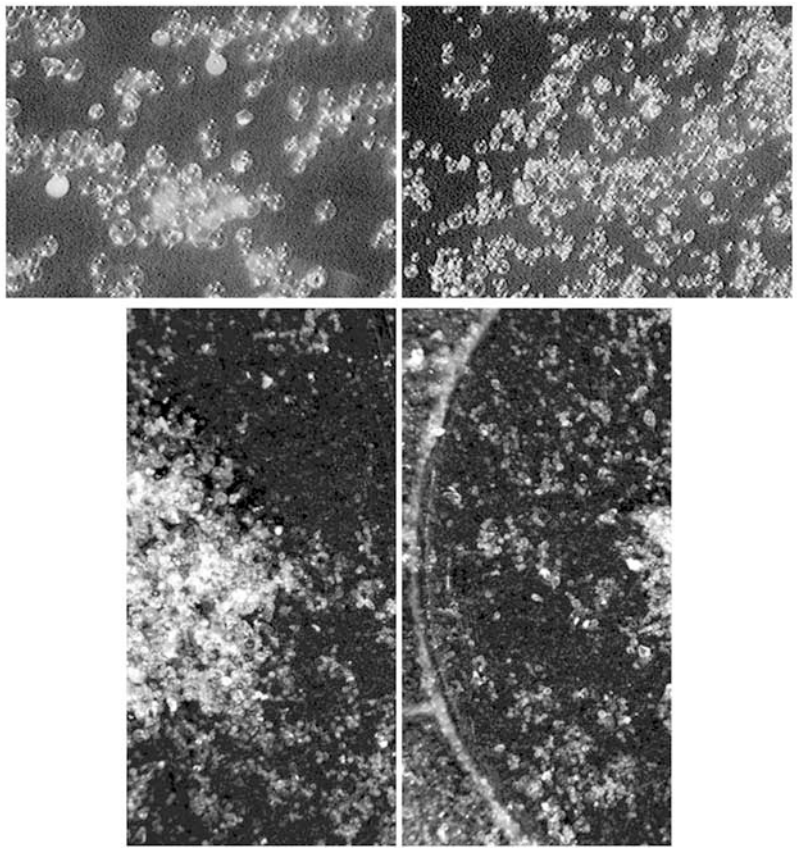

Figure 36. (top) Conventional microscopy images of (left) 10–53 μm and (right) 44–74 μm ballotini. The field of view is 1.5 mm horizontal. (bottom) Images (2 mm high by 1 mm wide) of the same samples from the OM test bed, rebinned to simulate the resolution and field of view of the flight camera.

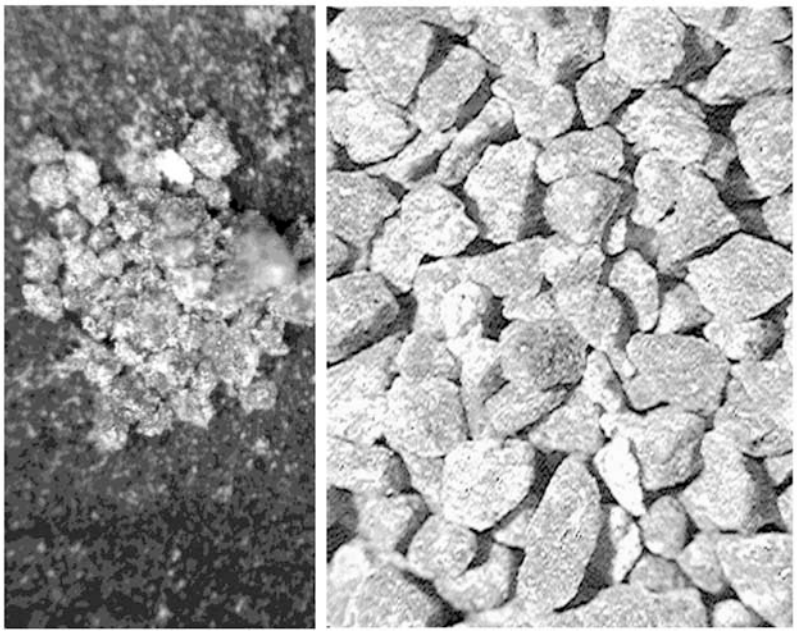

Figure 37. Angular crushed turbidite mudstone. (left) OM test bed image on magnet, 2 mm high $\times$ 1 mm wide. (right) Conventional high-resolution microscopy image, 1 mm high. Sample grains are $\sim$100 μm.

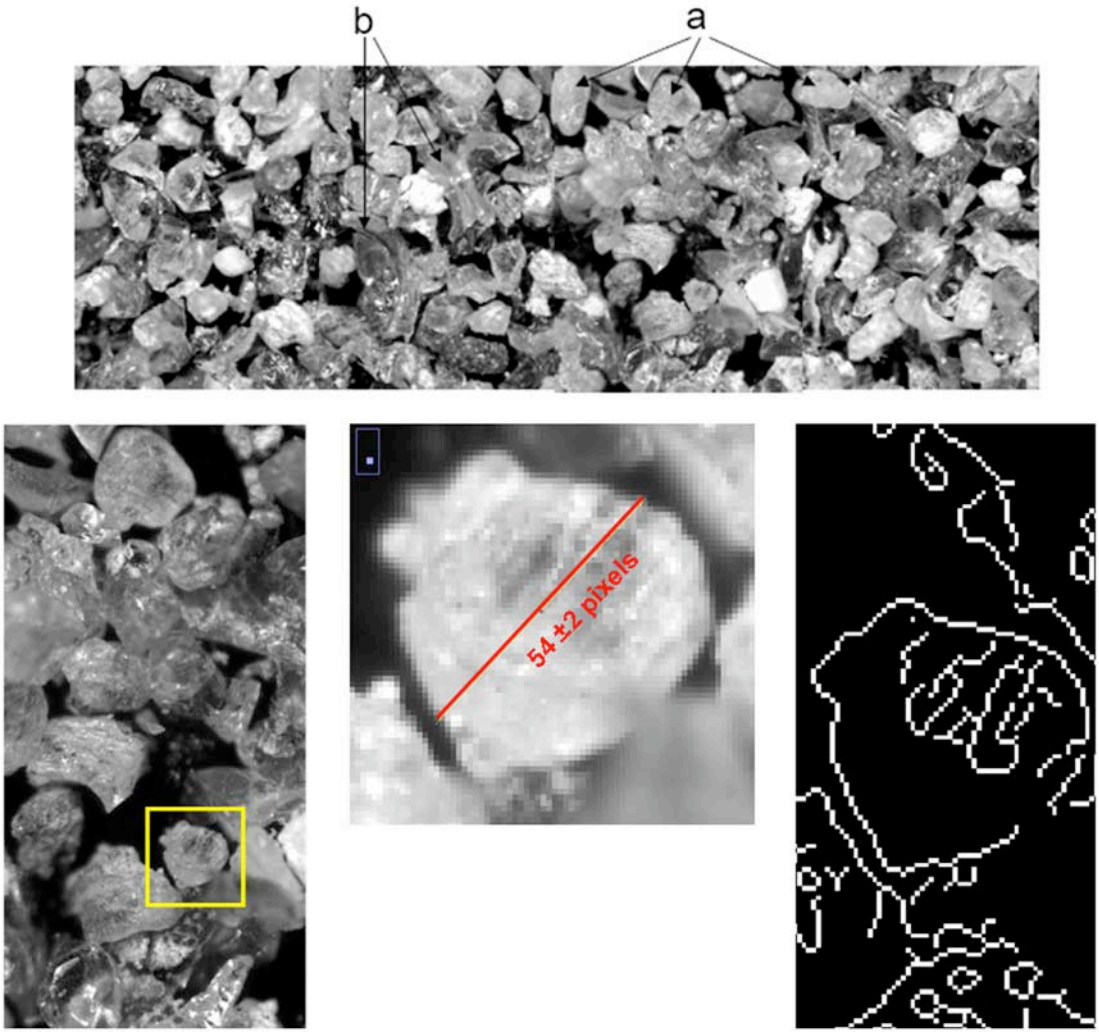

Figure 38. (top) Four frame mosaic of 177–250 μm grains. Bishop phreatomagmatic (Plinian) glass pyroclastic particles reworked on a low-energy lacustrine shoreline. Note presence of both well-rounded and frosted grains (noted by the a) mixed with angular clear vesicle shards (noted by the b), implying two distinct grain populations. (bottom left) OM image of an ensemble of 177–250 μm particles. A 200 μm particle has been (bottom middle) enlarged and (bottom right) measured with an edge detection routine.

quantify the shape of the grains, it is nevertheless clear that the material is not rounded, and that it has fine particulates parasitically clinging to the larger grains. Although the grains appear angular under the conventional microscope, this was not easy to determine at the resolution of the OM. Both the conventional and OM image indicate that the grains are ~100 um in diameter.

[85] To determine the size resolution of particles near the upper limit of acceptance by the sampling system, samples of Bishop phreatomagmatic (Plinian) glass pyroclastic particles reworked on a low-energy lacustrine shoreline were sieved to limit the population to 177–250 μm grains, corresponding to a standard sieve size. The sample was imaged by attaching the particles to a substrate with double-sided tape. Figure 38 shows a mosaic of four images. Both larger and smaller grains can be seen with great clarity – the OM can image (and resolve the size and shape of) 200 μm grains, even though the full grain is not in focus at any one focal position. Moreover, a single focal position captures

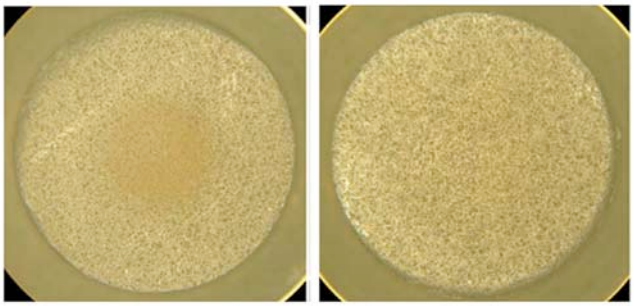

Figure 39. Images of the (left) strong and (right) weak magnets (conventional camera) after dusting with Salten Skov Mars analog.

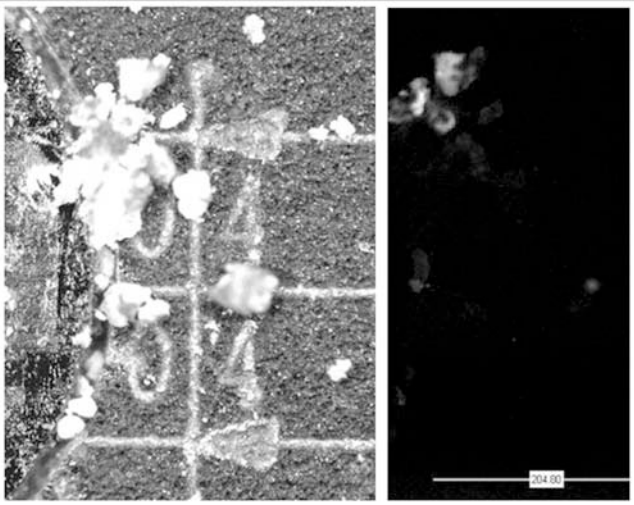

Figure 40. (left) Visible image of soap powder grains (full-resolution mode). (right) UV image of same grains highlighting fluorescent component (flight simulation mode).

the grain periphery sufficiently well to define both size and shape. Angular and rounded grains are very distinct (the sample was chosen for having both), and even the volcanic origin and glassy nature of the grains can be resolved. Also resolved is frosting (abrasion) on the surfaces of the well-rounded grains. Figure 38 also shows a 200 μm particle both measured directly and with an automatic edge-detection routine. The measurements are in agreement to within 2 pixels.

[86] Limited testing has been performed with magnetic substrates. In all tests to date with the flight-like OM both weak and strong magnets attract more material than other substrates, retain larger particles, and scavenge material that has not adhered to other substrates. This can be seen in Figure 39, where the sample has been deposited from a dusting chamber. More detail can be found elsewhere in this issue [*Leer et al.*, 2008]. It remains to be shown, however, whether the scavenged material is different in magnetic properties from material on other substrates. This will be the subject of further investigation.

[87] The fluorescence detection capability of the OM is not intended to be definitive or quantitative, but rather to determine whether further investigation of fluorescent properties of Martian soil is likely to be a fertile area of research. The technique takes advantage of the fact that the CCD is blind in the passband of the filter on the UV LED, and thus any particles visible under UV illumination must be fluorescing in the visible. To test this capability, particles of commercial laundry soap were used as a test sample, as fluorescent dye or ''blueing'' is commonly added to such detergent to make clothes look whiter in bright light. For comparison purposes, images were acquired of known nonfluorescent materials. Figure 40 shows visible and UV-illuminated images of the soap powder, clearly indicating a group of fluorescent grains in the upper left. No such fluorescence was observed from the control sample.

9. Operational Protocols

[88] The MECA Microscopy Station will evaluate samples of Martian dust and soil delivered either by the Phoenix Robotic Arm or directly deposited from the air. The first sample to be analyzed will be dust collected during landing, and will presumably represent surface material disturbed by the landing jets. In preparation for that event, four of the target substrates have been imaged in cruise (Figure 41) in order to verify their cleanliness and identify specific features (such as the fiber on the micromachined substrate) that should not be ascribed to the sample. Prior to landing they will be rotated and translated to the sample acquisition position.

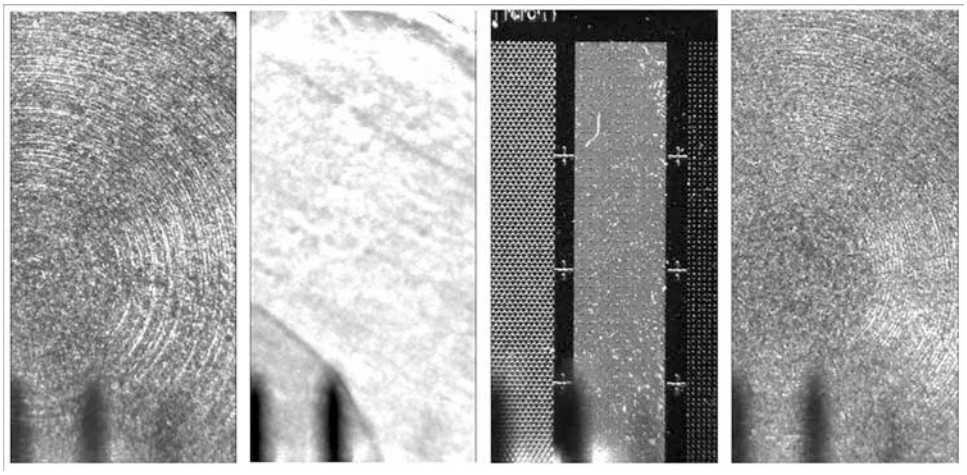

Figure 41. Monochrome OM images acquired in cruise of substrates that will be exposed during landing for (left) targets 59 (weak magnet), (left middle) 60 (silicone), (right middle) 61 (micromachined), and (right) 63 (strong magnet). Two AFM tips and their shadows can be seen out of focus in the foreground. The fiber on the micromachined substrate was present at integration but could not easily be removed without damaging the substrate. The remainder of the set, the microbuckets in targets 58 and 62, were not imaged since the bottom cannot be brought into focus when they are empty.

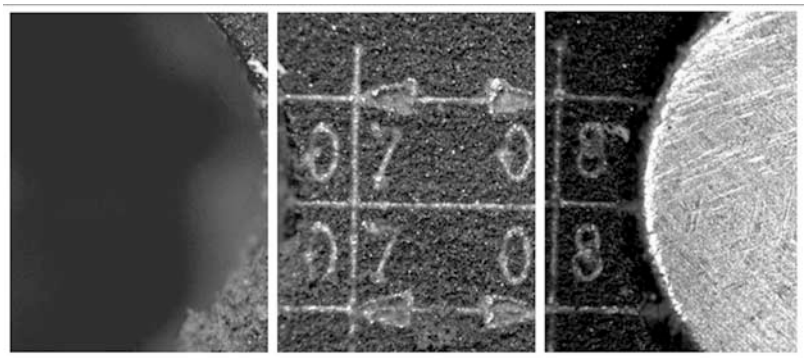

Figure 42. This triptych of images demonstrates that cross contamination is negligible on the "trailing" substrate set except for a few particles on (left) the edge of the microbucket. (right) The strong magnet, and (middle) the laser-etched space between the substrates.

[89] To operate the Microscopy Station, soil samples are deposited by the RA (or gravitationally from the air) onto a segment of the SWTS ring that has been extended such that exactly one set of 6 substrates protrudes from a horizontal slot in the MECA enclosure. Excess material is removed by passing the substrates under a blade positioned 0.2 mm above the surface. The exposed substrates are then rotated from their horizontal load positions into their vertical imaging positions.

[90] Attempting to scan excessively steep or ragged surfaces with the AFM will result in scans that are largely out of range, and could conceivably damage the AFM tip. Further, bandwidth and time constraints severely limit the number of scans that can be acquired and returned to Earth. These considerations dictate a two-day imaging strategy for each set of microscopy samples. On the first day the substrates are first inspected for cleanliness and any necessary instrument calibrations are performed. A sample is delivered, then characterized by the optical microscope. AFM calibration scans are also acquired. These images are evaluated on the ground and targets for AFM scanning are selected. On the second day the targeted areas are imaged again with the optical microscope, and then scanned with the AFM.

[91] The threat of cross contamination on sample delivery has been mitigated in part by extensive baffling of the inlet port, and is further compensated by pre-inspection of the targets before sample introduction. The tendency of the magnetic substrates to scavenge stray particles has also been exploited to prevent excessive dispersal of stray material during sample introduction. As the wheel is rotated from the sampling to the imaging position, small amounts of material spill forward onto previously used substrates (the first substrates used are adjacent to the notch in the wheel and therefore will not contaminate unused substrates). To prevent excessive dispersal of this material, the first substrate the falling particles encounter is a microbucket and the second is the strong magnet, intended to capture any particles that do not fall into the bucket. The effectiveness of this method was demonstrated using a fine grained (<1 mm) salt poor, initially water rich basaltic tephra, one of several analogs prepared for the Phoenix mission by Dr. Richard Morris of the NASA Johnson Space Center. Prior to testing, the sample was preheated at 65C for 1.5 h in a desiccated vessel. Like all mineralogical samples tested, the fine particles from this sample adhere preferentially to the strong magnet. After deposition of the sample the wheel was slowly retracted into the enclosure, then rotated toward the observation position. Figure 42 shows the pristine substrates trailing the targeted set during the rotation. The images show that the microbucket buffer acquired a small amount of material, but the next substrate is particle-free. Figure 43 shows a mosaic of the surface of the strong magnet from the substrate set in the leading direction, which

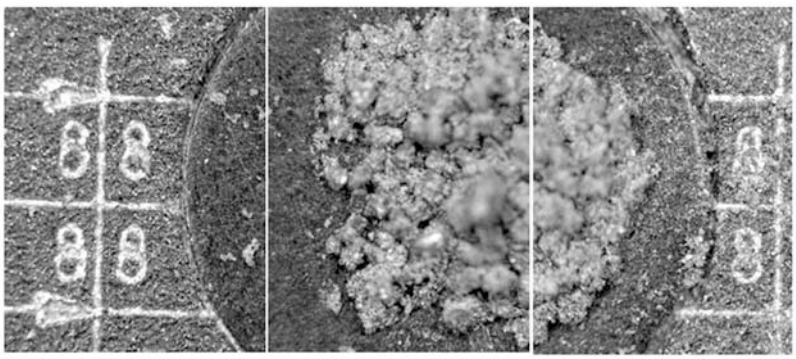

Figure 43. A mosaic of images showing cross contamination near the center of the magnet on the "leading" substrate set but not in the surrounding areas.

Figure 44. Combined red, green, and blue image of nanobucket substrate acquired on a test bed at Imperial College. The blue object in the lower left corner and the purple band are artifacts of specular reflection from silicon crystal surfaces. The particles, however, are a realistic color and stand out clearly in contrast.

receives the bulk of the contamination. In this case the microbucket buffer was insufficient to trap the spillage, and a significant amount was trapped on the magnet. However, none of the substrates to the left of the magnet were contaminated.

[92] Shortly after acquisition, all Phoenix data products will be archived in the Planetary Data System in both raw and processed form. The optical microscope data products include color images (Figure 44), fluorescence images (Figure 40), mosaics of adjacent fields (Figure 30), and through-focus series of images (Figure 27). Bandwidth limits require JPEG compression, typically from 4:1 to 12:1. AFM data products include large area topographs that can be compared to sections of OM images, and automatically zoomed topographs centered within the large area (Figure 16).

10. Discussion and Conclusions

[93] The objective of the microscopic examination of Martian soil is to characterize the particle type and to acquire some sense of its history by examination of particle size distribution, shape, and texture, as well as characteristics such as color, homogeneity, and particle-particle interactions (aggregation). From size characterization one can deduce whether the surface particles consist primarily of dust deposited by wind or altered regolith material. From shape characterization one can deduce, for example, whether comminution or chemical erosion was the dominant process. For example, particles of micrometer size do not get rounded mechanically owing to limits of Griffith flaw spacing, and the fact that particles with such low Reynolds numbers do not collide with much force, and tend to follow fluid flow directions because they respond to viscous rather than inertial forces. If the fines in a sediment are rounded, it is therefore likely that the cause is chemical, strongly implicating the presence of water at some stage but not excluding the action of atmospheric oxidants. Very angular fine particles, on the other hand, particularly from depth in the soil, would indicate that the soil had not experienced either aqueous transport or weathering processes.

[94] Combined with contextual information from RAC imaging and TECP measurements of thermal properties, particle size and shape distributions can allow for some estimation of soil porosity and tortuosity, which in turn determine the diffusive properties of the regolith with respect to heat and water vapor. These are important parameters for modeling the response of the regolith to climate history. Establishing a limit to soil porosity is particularly relevant to the interpretation of the data from Odyssey's Gamma Ray Spectrometer (GRS), which suggests an extraordinarily large ice volume fraction just beneath the surface. A finding that the porosity of the overlying soil is significantly different from that of the underlying permafrost would suggest that vapor diffusion alone is not responsible for the formation of the ice.

[95] Secondarily, one can look at adhesion processes as a clue to the evolution of regolith structure. The importance of electrostatic interactions can be inferred both from observed particle-particle interactions and from particle-substrate interactions. The magnetic properties of particles can be studied by characterizing the deposits on the magnetic substrates [see *Leer et al.*, 2008]. Note that the direct observation of ice particles per se is not a specific objective of the microscopy experiment. At particle sizes of 0.1 mm and below, the lifetime of isolated ice particles at the operating temperature of the microscope is limited to tens of minutes.

[96] The AFM is intended to expand the detail of particles and features seen in the OM images and to provide the relevant three-dimensional topography. It has been included in the microscopy suite to address the study of airborne particles, which are typically in the size range of a few μm, and to characterize μm−scale textures and fractures on larger particles.

[97] With the landing of Phoenix in May 2008, the MECA Microscopy Station will offer several firsts in Mars exploration. The unprecedented resolution of the microscope will acquire the first-ever images of airborne dust particles. Of particular interest will be clues to the evolution of the particle ensembles provided by particle shapes and distributions, and electrostatic interactions between particles, such as the formation of particle chains that might

lead to their precipitation. The ability to introduce samples into a darkened enclosure allows MECA to acquire fluorescent images of Martian particles for the first time. Microscopy Station images will address questions of particle homogeneity associated with magnetic and, in concert with the MECA wet chemistry laboratory, chemical properties. Finally, MECA will pioneer the first-ever extraterrestrial use of atomic force microscopy.

[98] **Acknowledgments.** The authors are indebted to Mike Ackeret, Judy Ackeret, Mark Balzer, Don Bickler, Chuck Bryson, Greg Cardell, Lynne Cooper, Niels Harrit, Bruno Jau, Kim Kuhlman, Morten Madsen, Korla McFall, Mike Newell, Phillippe Niedermann, Joel Rademacher, Robert Reynolds, Mitch Shellman, Mike Shirbacheh, Lisa Tatge, Kevin Watson, Eugenius Zych, numerous other members of the MECA and Phoenix development teams who contributed immeasurably to this work, the staffs of the various vendors and academic partners who contributed hardware components to this experiment, and our scientific colleagues who provided test samples, reviewed our work plans, and are instrumental in the planning of MECA operations on Mars. This work would not have been possible without generous international contributions of the AFM from Switzerland, the OM detector system from Germany, micromachined substrates from the UK, and both magnetic substrates and UV calibration targets from Denmark. The sponsors of those components are gratefully acknowledged. The balance of the research described in this publication was performed under contract with the National Aeronautics and Space Administration, including those portions performed at the Jet Propulsion Laboratory, California Institute of Technology, and at the University of Arizona.

References

Akiyama, T., et al. (2001), Atomic force microscope for planetary applications, *Sens. Actuators*, *91*, 321–325.

Gautsch, S. (2002), Development of an atomic force microscope and measurement concepts for characterizing Martian dust and soil particles, Ph.D. thesis, Univ. of Neuchâtel, Neuchâtel, Switzerland.

Gautsch, S., et al. (2002), Measurement of quartz particles by means of an atomic force microscope for planetary exploration, *Surf. Interface Anal.*, *33*, 163–167, doi:10.1002/sia.1182.

Hecht, M. H., et al. (1999), The MSP '01 Mars Environmental Compatibility Assessment (MECA), paper presented at 5th International Conference on Mars, NASA, Pasadena, Calif., 18–23 Jul.

Keller, H. U., et al. (2008), The Phoenix Robotic Arm Camera, *J. Geophys. Res.*, doi:10.1029/2007JE003044, in press.

Kempe, A., F. Jammitzky, W. Altermann, B. Baisch, T. Markert, and W. M. Heckl (2004), Discrimination of aqueous and aeolian paleo environments by atomic force microscopy—A database for the characterization of Martian sediments, *Astrobiology*, *4*, 51–64, doi:10.1089/153110704773600221.

Kramm, J. R., N. Thomas, H. U. Keller, and P. H. Smith (1998), The CCD imager electronics for the Mars Pathfinder and Mars Surveyor cameras, *IEEE Trans. Instrum. Meas.*, *47*(5), 1112–1118, doi:10.1109/19.746566.

Leer, K., P. Bertelsen, C. S. Binau, L. Djernis Olsen, L. Drube, T. V. Falkenberg, M. P. Haspang, M. B. Madsen, and M. Olsen (2008), Magnetic properties experiments and the SSI calibration target onboard the Mars Phoenix 2007 Lander: Design, calibration, and science goals, *J. Geophys. Res.*, *113*, E00A16, doi:10.1029/2007JE003014.

Marshall, J. R., et al. (1999a), The MECA payload as a dust analysis laboratory on the MSP 2001 Lander, *Proc. Lunar Planet. Sci. Conf.*, *XXXth*, abstract 1163.

Marshall, J. R., et al. (1999b), The MECA payload as an exobiology laboratory on the MSP 2001 Lander, *Proc. Lunar Planet. Sci. Conf.*, *XXXth*, abstract 1164.

Marshall, J. R., K. Kuhlman, R. Stevens, and M. Meyyappan (2001), Study of a Martian aeolian analog with MECA microscopy, *Proc. Lunar Planet. Sci. Conf.* [CD-ROM], *32*, abstract 1265.

Pike, W. T., M. H. Hecht, P. H. Smith, and U. Staufer (2001), A microscopy stage for Mars, paper presented at Electron Microscopy and Analysis Group Conf., Inst. of Phys., Dundee, UK.

Thomas, N., et al. (2004), The Microscope for Beagle 2, *Planet. Space Sci.*, *52*, 853–866, doi:10.1016/j.pss.2004.02.008.

Vijendran, S., H. Sykulska, and W. T. Pike (2007), AFM investigation of Martian soil simulants on micromachined Si substrates, *J. Microsc.*, *227*(3), 236–245, doi:10.1111/j.1365-2818.2007.01806.x.

Zych, E., W. Goetz, N. Harrit, and H. Spanggaard (2004), Spectroscopic properties of sintered $BaMgAl_{10}O_{17}:Eu^{2+}$ (BAM) translucent pellets: Comparison to the commercial powder, *J. Alloys Compd.*, *380*, 113–117, doi:10.1016/j.jallcom.2004.03.036.

D. Blaney, M. H. Hecht, A. Mazer, C. Mogensen, J. M. Morookian, and M. Weilert, Jet Propulsion Laboratory, California Institute of Technology, 4800 Oak Grove Drive, Pasadena, CA 91109, USA. (michael.h.hecht@jpl.nasa.gov)

D. Braendlin, Nanosurf AG, Grammetstrasse 14, CH-4410 Liestal, Switzerland.

S. Gautsch, D. Parrat, and U. Staufer, Institute of Microtechnology, University of Neuchâtel, A.-L. Breguet 2, CH-2000 Neuchâtel, Switzerland.

W. Goetz, H. U. Keller, and W. J. Markiewicz, Max Planck Institute for Solar System Research, Max-Planck- Strasse 2, D-37191 Katlenburg-Lindau, Germany.

H.-R. Hidber and A. Tonin, Department of Physics, University of Basel, St. Peter's Square 1, CH-4003 Basel, Switzerland.

J. Marshall, SETI Institute, 515 North Whisman Road, Mountain View, CA 94043, USA.

T. P. Meloy, College of Engineering and Mineral Resources, West Virginia University, 413 Jefferson Street, Morgantown, WV 26501, USA.

W. T. Pike, H. Sykulska, and S. Vijendran, Department of Electrical and Electronic Engineering, Imperial College, Exhibition Road, South Kensington, London SW7 2DD, UK.

R. O. Reynolds, P. Smith, R. J. Tanner, and P. M. Woida, Lunar and Planetary Laboratory, University of Arizona, Tucson, AZ 85721, USA.